Journal Pre-proofs

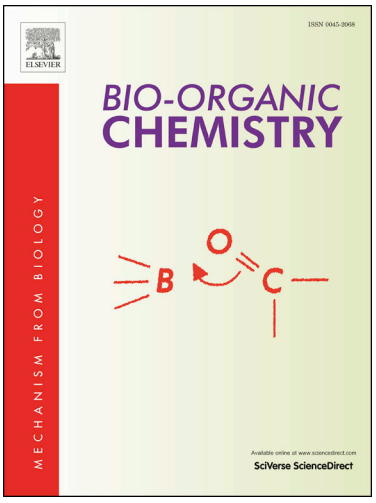


# Identification and structure-activity relationship (SAR) studies of carvacrol derivatives as potential anti-malarial against *Plasmodium falciparum* Falcipain-2 protease

Amad Uddin, Vigyasa Singh, Iram Irfan, Taj Mohammad, Rahul Singh Hada, Md Imtaiyaz Hassan, Mohammad Abid, Shailja Singh

PII: S0045-2068(20)31439-5
DOI: https://doi.org/10.1016/j.bioorg.2020.104142
Reference: YBIOO 104142

To appear in: *Bioorganic Chemistry*

Received Date: 3 May 2020
Revised Date: 30 June 2020
Accepted Date: 23 July 2020

Please cite this article as: A. Uddin, V. Singh, I. Irfan, T. Mohammad, R. Singh Hada, M. Imtaiyaz Hassan, M. Abid, S. Singh, Identification and structure-activity relationship (SAR) studies of carvacrol derivatives as potential anti-malarial against *Plasmodium falciparum* Falcipain-2 protease, *Bioorganic Chemistry* (2020), doi: https://doi.org/10.1016/j.bioorg.2020.104142

# Identification and structure-activity relationship (SAR) studies of carvacrol derivatives as potential anti-malarial against *Plasmodium falciparum* Falcipain-2 protease

**Amad Uddin[1, 2‡], Vigyasa Singh[2‡], Iram Irfan[1], Taj Mohammad[3], Rahul Singh Hada[4], Md Imtaiyaz Hassan[3], Mohammad Abid[1*] and Shailja Singh[2*]**

[1]*Medicinal Chemistry Laboratory, Department of Biosciences, Jamia Millia Islamia, Jamia Nagar, New Delhi, 110025, India*
[2]*Special Centre for Molecular Medicine, Jawaharlal Nehru University, New Delhi, 110067, India*
[3]*Center for Interdisciplinary Research in Basic Sciences, Jamia Millia Islamia, Jamia Nagar, New Delhi-110025, India*
[4]*Department of Life Sciences, Shiv Nadar University, Gautam Buddha Nagar UP, 201314, India*

✉To whom correspondence should be addressed**:** mabid@jmi.ac.in (M. Abid), shailja.jnu@gmail.com (S. Singh).

‡These authors contributed equally to this work.

**Abstract:** In an effort to develop a potent anti-malarial agent against *Plasmodium falciparum*, a structure-guided virtual screening using an *in-house* library comprising 652 compounds was performed. By docking studies, we identified two compounds (**JMI-105** and **JMI-346**) which formed significant non-covalent interactions and fit well in the binding pocket of *Pf*FP-2. We affirmed this observation by MD simulation studies. As evident by the biochemical analysis, such as enzyme inhibition assay, Surface Plasmon Resonance (SPR), live-cell imaging and hemozoin inhibition, **JMI-105** and **JMI-346** at 25µM concentration showed an inhibitory effect on purified *Pf*FP-2. **JMI-105** and **JMI-346** inhibited the growth of $CQ^S$ (3D7; $IC_{50}$ = 8.8 and 13µM) and $CQ^R$ (RKL-9; $IC_{50}$ = 14.3 and 33µM) strains of *P. falciparum*. Treatment with compounds resulted in defect in parasite growth and development. No significant hemolysis or cytotoxicity towards human cells was observed suggesting that these molecules are non-toxic. We pursued, structural optimization on **JMI-105** and in the process, SAR oriented derivatives (**5a-5l**) were synthesized and evaluated for growth inhibition potential. **JMI-105** significantly decreased parasitemia and prolonged host survival in a murine model with *P. berghei* ANKA infection. The compounds (**JMI-105** and **JMI-346**) against *Pf*FP-2 have the potential to be used as an anti-malarial agent.

**Keywords:** *Plasmodium falciparum;* Malaria; Falcipain-2; Virtual screening; SAR studies.

## 1. Introduction

Malaria is one of the most endemic tropical parasitic diseases, caused by blood born Apicoplexan parasite *Plasmodium falciparum* (*P. falciparum*) around the world [1, 2]. It is responsible for about one million deaths annually [3, 4]. Five species of *Plasmodium* out of 200 known ones are able to infect human, which includes *P. falciparum*, *P. vivax*, *P. ovale*, *P. knowelsi* and *P. malariae*. *P. falciparum* is the most lethal one and responsible for over 95% cases worldwide [5]. Irrespective of the efforts made to control malaria under the eradication programs, in 2018, the World Health Organization (WHO) estimated 228 million cases worldwide, and 4,05,000 death [6]. The emergence and spread of the resistance to the commonly available and inexpensive drugs limited the efficiency of anti-malarial therapies resulting in an increase of the mortality rate [7]. To combat spread of multidrug-resistance in *P. falciparum*, the WHO recommended Artemisinin based Combination Therapies (ACTs). However, there have been reports on decreased susceptibility of the parasite to artemisinins in the Greater Mekong Subregion (GMS), followed by ACTs' failure leading to a worrisome situation. [8]. Therefore, it becomes imperative to explore newer strategies for the control and eradication of malaria.

Proteases of *P. falciparum* act are the attractive target for most of the drugs playing crucial role in growth, and development of the parasite during its life cycle [9]. A complete genome of *P. falciparum* consists of 33 open reading frames that encode cysteine proteases and a family of four cathepsin L-like papain proteases collectively known as falcipains [10]. Falcipain-2 (*Pf*FP2) and falcipain-3 (*Pf*FP3) are key papain-family (C1) Clan CA trophozoite cysteine proteases which lies in the digestive food vacuole that cleaves host hemoglobin (native and denature) and also responsible for erythrocyte rupture. The inflation of malarial parasite inside the infected red blood cell is proportionate to rate of its food assimilation [11]. Cysteine proteases of *Plasmodium* are implicated with several biological processes like, rupture of membranes, degradation of Hb, protein trafficking and host cell invasion [12, 13]. Thus, the growth of malarial parasites is measured by the interference of key indicator protein *Pf*FP2 [14]. Among falcipains, the most expressed and well-studied one is *Pf*FP2 which is an attractive target for the discovery of antimalarial drug [15].

Virtual screening methods have helped in identifying new leads for drug development [16-18]. Structure-based virtual screening (SBVS) is commonly used for the identification of

potential compounds preferentially binding to a drug target [19]. SBVS involves computational methods, including molecular docking and dynamic simulations of receptor-ligand and their complexes [20]. First, the compounds were screened based on their binding affinities and predicted interactions with the target and those with the higher scores (hits) were selected for experimental activity assays. The availability of the X-ray crystal structure of *Pf*FP2 in complex with its known inhibitor E64 (PDB ID: 3BPF) opened newer avenue to discover its inhibitors through structure-based virtual screening of natural/synthetic libraries as potent anti-malarials. In the present study, an in-house library of 652 compounds was screened through DruLiTo for their likelihood of drug molecules based on their physicochemical and ADMET properties. The selected compounds were evaluated for their ADME/T properties. Further, we used AutoDock Vina to identify high-affinity binding partners of *Pf*FP2 by utilizing molecular docking approach. The compounds showing high binding affinity towards *Pf*FP2 were selected further for interaction analysis and molecular dynamics (MD) simulations. We identified two compounds (**JMI-105** and **JMI-346**) as potential *Pf*FP2 inhibitors and subjected them to various biochemical studies. This included growth inhibition, live-cell imaging and cytotoxicity assays and *in vivo* studies for their evaluation as potential anti-malarials.

## 2. Results and Discussion

### *2.1. In silico studies*

*In silico* studies were conducted in search of antimalarial compounds by using different bioinformatics tools encompassing AutoDock Vina [21], PyRX and Discovery Studio [22], PyMOL [23], online resources such as RCSB Protein Data Bank, SwissADME [24], CarcinoPred-EL [25], MGL Tools [26], VMD (Visual Molecular Dynamics), QtGrace [27] and GROMACS [28]. These were used for data visualization, data retrieval, evaluation, and molecular dynamics (MD) simulations.

#### *2.1.1. Drug-likeliness assessment of In-house library*

The Lipinski's criteria generally referred to as the "Rule of Five" (Ro5), which has been used as a part of the assessment of presumable oral accessibility of the selected compounds. Thus, the drug-potential of selected compounds was assessed by calculating the Lipinski's Ro5 descriptors. Out of 652 compounds, a total of 46 fulfilled all the Ro5 criteria showing well defined physicochemical properties of which 17 were selected. The physicochemical properties

of the selected compounds are listed in (Supplementary data), while two of the selected compounds **JMI-105** and **JMI-346** and their physicochemical properties are shown in **Table 1**. Both compounds are showing drug-like properties following the Lipinski's rule of five.

**Table 1:** Physicochemical properties of **JMI-105** and **JMI-346** compounds

| Compound ID | Mol. Weight | HBD | Rotatable bond | HBA | Log P | Lipinski Violation |
|---|---|---|---|---|---|---|
| **JMI-105** | 337.18 | 0 | 6 | 5 | 3.69 | 0 |
| **JMI-346** | 336.16 | 1 | 7 | 6 | 2.15 | 0 |

On the basis of ADMET predictions, selected compounds were further filtered out. Out of 17 compounds, 12 were showing favorable ADMET properties (Supplementary data). All these compounds were found to be non-carcinogenic as predicted through Carcinopred-EL. ADMET properties and carcinogenicity of compounds **JMI-105** and **JMI-346** mentioned in (**Table 2**).

**Table 2:** ADMET properties of **JMI-105** and **JMI-346** compounds

| Compound ID | logD | logS | Rigid Bond | F | Solubility (mg/l) | C Atoms | Ratio H/C | Carcinogen |
|---|---|---|---|---|---|---|---|---|
| **JMI-105** | 4.93 | -4.51 | 17 | 0.26 | 3698.60 | 20 | 0.25 | NC |
| **JMI-346** | 3.11 | -3.33 | 18 | 0.28 | 12031.2 | 19 | 0.32 | NC |

### *2.1.2. Molecular docking*

Molecular docking of 12 compounds showed discernible binding affinity with *Pf*FP-2 than with *Pf*FP-3. The possible confirmations of 12 selected compounds were generated using Vina Split program. A total of 108 docked confirmations of 12 selected compounds were subjected to interaction analysis towards *Pf*FP-2 and *Pf*FP-3 (Supplementary data). Out of 12 compounds, **JMI-105** and **JMI-346** showed binding affinity with *Pf*FP-2, calculated as -7.5 kcal/mol and -7.3 kcal/mol, respectively. These compounds showed binding with the ligand-binding site of FP-2 interacting with several important residues of *Pf*FP-2. The interactions of **JMI-105** and **JMI-346** compounds along with E-64 (Co-crystallized ligand) are shown in

(**Table 3**). The interaction analysis suggests that both compounds occupy the same position of FP-2 binding site mimicking the binding pose of each other (**Fig. 1A**). The ***Pf*FP-2-JMI-105** and ***Pf*FP-2-JMI-346** complexes stabilized by 3-4 hydrogen bonds showing several other significant interactions (**Fig. 1B, 1C**).

**Table 3.** Molecular interaction of **JMI-105, JMI-346** and E-64 (Co-crystallized ligand) with *Pf*FP-2 binding site

| **Comp ID** | **Compound structure** | **Protein-ligand Interaction** | | | |
|---|---|---|---|---|---|
| | | **Affinity (kcal/mol)** | **Hydrogen Bond** | | **Other Interacting Residues** |
| | | | **Residues** | **Distance (Å)** | |
| **JMI-105** | 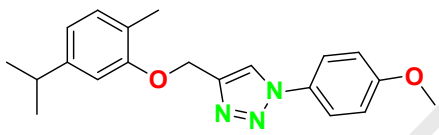 | -7.5 | Lys37 Asp35 Trp206 | 3.08, 2.85, 2.93 | Ala157, Trp210, Ser205, Lys37, Asn173, Gln36, Val152, Asn38, His174 |
| **JMI-346** | 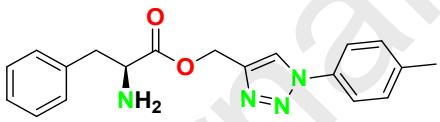 | -7.3 | Gln36 Trp206 | 3.09, 3.25, 3.02 | Gly209, Lys37, Asp35, His174, Cys42, Asn173, Gly82, Asn81, Ala157 |
| **E-64** | 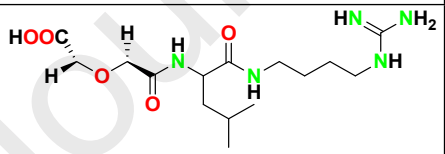 | -5.1 | His174 Trp206 | 2.92, 2.82 | Gln36, Ala157, Phe158, Trp210, Asn173 |

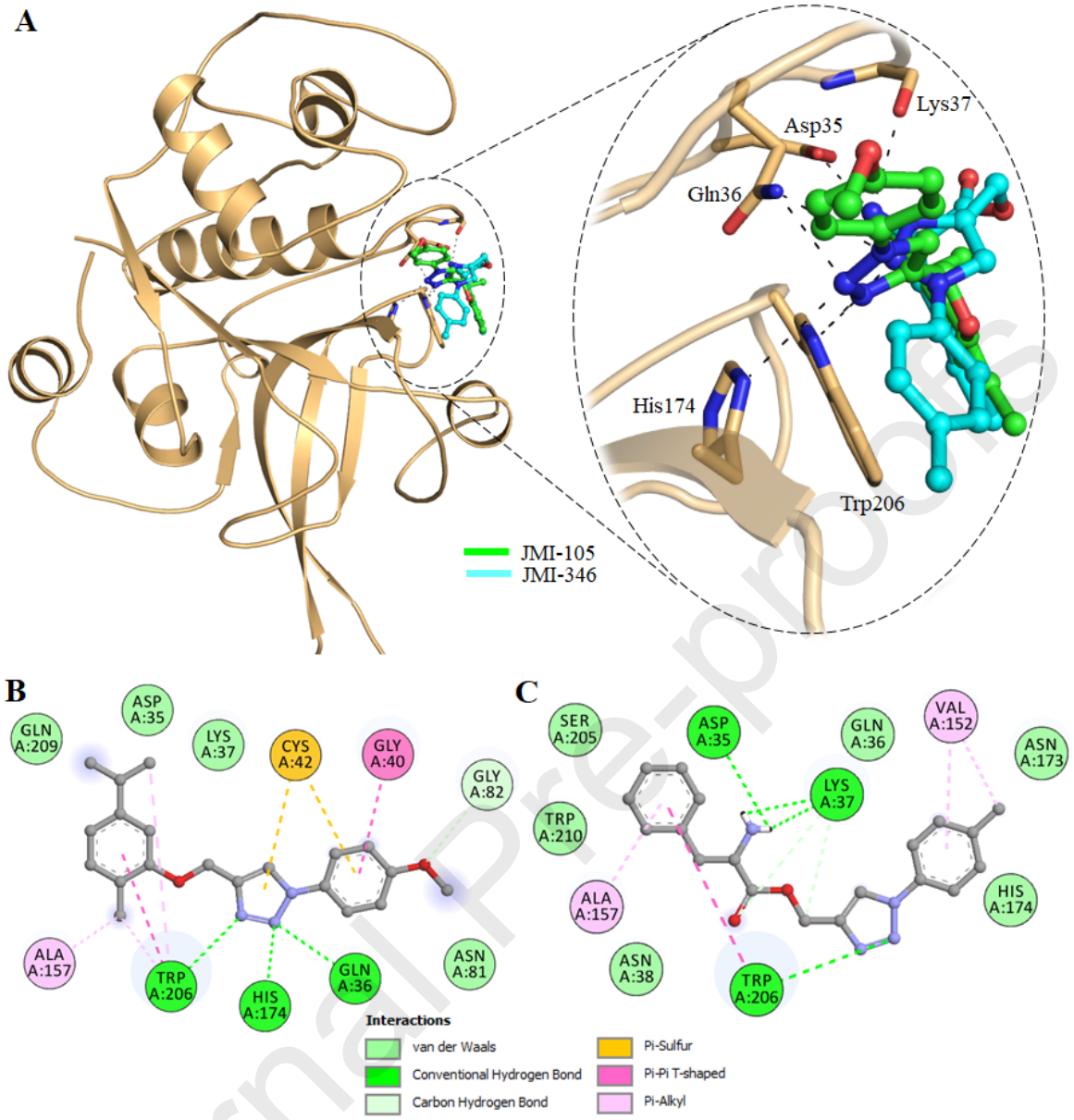


**Figure 1:** Structural organization of *Pf*FP-2 with **JMI-105** and **JMI346. (A)** Cartoon representation of *Pf*FP-2 showing the docked **JMI-105** and **JMI-346**. Zoomed view of *Pf*FP-2 binding site with **JMI-105** and **JMI-346** (right panel). (**B**) 2-D representation *Pf*FP-2 residues interacting to **JMI-105** and (**C**) **JMI-346**.

### *2.1.3. MD simulations*

MD simulations technique has been widely used to assess the internal motion, physical arrangements and environmental-induced structural changes in proteins and their interactions with other chemical molecules [47]. MD simulations can describe the dynamics of the binding mechanism of a small molecule to a protein under an explicit solvent surroundings [48]. Here,

we performed all-atom MD simulations of free *Pf*FP-2 and **JMI-105** and **JMI-346** docked complexes of *Pf*FP-2 for 30 ns to evaluate the conformational changes, stability and interaction mechanism. Average potential energies of free *Pf*FP-2, *Pf*FP-2-**JMI-105** and *Pf*FP-2-**JMI-346** complexes were calculated to ascertain the equilibration and stability of the systems prior to MD analysis. The potential energy of free *Pf*FP-2, *Pf*FP-2-**JMI-105** and *Pf*FP-2-**JMI-346** systems was calculated as -9,10,842 kJ/mol, -9,10,083 kJ/mol and -9,10,066 kJ/mol, respectively. The volume, density, kinetic energy, enthalpy, and total energy of the systems were also calculated over the simulations (**Table 4**).

**Table 4:** Calculated parameters for all three systems obtained after 30 ns MD simulations.

| System | RMSD (nm) | RMSF (nm) | Rg (nm) | SASA ($nm^2$) | Kinetic energy | Enthalpy | Volume ($nm^3$) | Density (g/l) |
|---|---|---|---|---|---|---|---|---|
| ***Pf*FP-2** | 0.13 | 0.08 | 1.72 | 129.30 | 1,43,282 | -763570 | 595.17 | 1,028.44 |
| ***Pf*FP-2-JMI-105** | 0.19 | 0.09 | 1.67 | 122.85 | 1,42,810 | -762364 | 588.91 | 1,029.51 |
| ***Pf*FP-2-JMI-346** | 0.24 | 0.12 | 1.73 | 113.48 | 1,46,460 | -762182 | 593.54 | 1,021.21 |

In the globular structure of a protein, the large conformational changes can occurs due to binding of a small molecule [49, 50]. The stability and evaluation of structural deviation can be determined by studying the Root mean square deviation (RMSD) of the structures [51]. The averages RMSD of free *Pf*FP-2, *Pf*FP-2-**JMI-105** and *Pf*FP-2-**JMI-346** complexes were found to be 0.13 nm, 0.19 nm and 0.24 nm, respectively (**Table 4**). The RMSD of all three systems do not show any significant change suggesting the stabilized binding of compounds with *Pf*FP-2 having fewer conformational changes (**Fig. 2A**). In RMSD plot, upon binding of compounds the random variation can be seen up to 10 ns, which may be due to their initial orientation in the binding pocket of *Pf*FP-2. Afterward, *Pf*FP-2 in the presence of **JMI-105** and **JMI-346** showed equilibration in RMSD throughout the simulation trajectory (**Fig. 2A**). The RMSD plot suggested enough stability of the protein-ligand complexes. The RMSD showed the *Pf*FP-2-**JMI-105** complex more compact and stable as compared to the *Pf*FP-2-**JMI-346** complex.

We plotted the root-mean-square fluctuation (RMSF) value of each residues to assess the residual flexibility present in free *Pf*FP-2 and *Pf*FP-2 in complex with **JMI-105** and **JMI-346** (**Fig. 2B**). The residual fluctuations were shown in RMSF plot at variable regions of the *Pf*FP-2

structure and stabilizations throughout the simulation. The average RMSF of free *Pf*FP-2 and in complex with **JMI-105** and **JMI-346** was obtained as 0.08 nm, 0.09 nm and 0.12 nm, respectively. Still, many increasing residual fluctuations can be seen after the binding of **JMI-346** with *Pf*FP-2, which might be due to the systematic vibrations in the protein during simulation. Fewer increased fluctuations in the *Pf*FP-2 after **JMI-346** binding was noticed which might be due to ligand adjustment in the binding pocket of the protein. The RMSF analysis also showed that the *Pf*FP-2-**JMI-105** complex is more compact and stable compared with *Pf*FP-2-**JMI-346**.

The structural parameters of a protein, such as tertiary volume and overall globular state can be signified by the radius of gyration ($R_g$) which is broadly used to analyze the protein's stability under biological environment [2]. The average values of $R_g$ for free *Pf*FP-2, *Pf*FP-2-**JMI-105** and *Pf*FP-2-**JMI-346** complexes were calculated as 1.72 nm, 1.67 nm and 1.73 nm, respectively. $R_g$ plot showed slight changes but no significant structural switching was observed in binding of *Pf*FP-2 packing with **JMI-105** and **JMI-346** compounds. *Pf*FP-2 in presence of **JMI-105** and **JMI-346** attained a higher $R_g$ as compared with free *Pf*FP-2, which is equilibrated throughout the simulations (**Fig. 2C**). The results showed a fewer structural deviation in *Pf*FP-2 upon binding with **JMI-105** and **JMI-346** compounds as no conformational shift was observed in the $R_g$ plot. While comparing both the complex systems, *Pf*FP-2-**JMI-105** is more compact and stable than *Pf*FP-2-**JMI-346**.

The surface area of a protein that is accessible to its surrounding solvent is termed as Solvent accessible surface area (SASA) which is precisely associated to the $R_g$ of a protein [51]. The SASA for free-*Pf*FP-2, *Pf*FP-2-**JMI-105** and *Pf*FP-2-**JMI-346** complex over the simulations was calculated. An average of SASA for *Pf*FP-2 protein alone and in complex with **JMI-105** and **JMI-346** were found to be 129.30 $nm^2$, 122.85 $nm^2$ and 113.48 $nm^2$, respectively. Change in SASA suggested few conformational adjustments in *Pf*FP-2 upon binding with **JMI-105** and **JMI-346** compounds (**Fig. 2D**). However, the SASA of *Pf*FP-2-**JMI-105** system attained a stable equilibrium without any switching during the entire simulation suggesting structural stability of *Pf*FP-2 in the presence of **JMI-105**. A decrease in SASA was observed in case of *Pf*FP-2-**JMI-346** possibly due to increased surface area of *Pf*FP-2 in presence of **JMI-346** where some outer residues might be buried to the inner core of the protein.

The protein stability is fundamentally determined by intramolecular hydrogen bonding. The stability of polar contact between a protein and ligand can also be evaluated by studying the

dynamics of Hydrogen bonds that can provide a direction, and specificity of protein-ligand interaction [52]. To further evaluate the stability of free-*Pf*FP2, *Pf*FP2-**JMI-105** and *Pf*FP2-**JMI-346** complex, hydrogen bonds paired within 0.35 nm were calculated over the simulations. An average number of intra-protein hydrogen bonds within *Pf*FP-2 before and after binding with **JMI-105** and **JMI-346** were found to be 160, 159 and 157, respectively **(Fig. 2E)**. A little decrement in hydrogen bonding within *Pf*FP2 itself might be due to the occupancy of some intramolecular space by the compounds. The analysis of hydrogen bond dynamics indicates that both complexes are quite stable with minimal change. While analyzing the dynamics of Hydrogen bonding between the compounds and the protein, an average of three hydrogen bonds were found between *Pf*FP-2-**JMI-105** and *Pf*FP-2-**JMI-346** throughout the simulations. It was observed that **JMI-105** and **JMI-346** bind in the binding site of *Pf*FP-2 with 5-6 conventional hydrogen bonds with higher fluctuations, and 3-4 hydrogen bonds with least fluctuations, which were consistent with our molecular docking findings (**Fig. 2 F-G**).

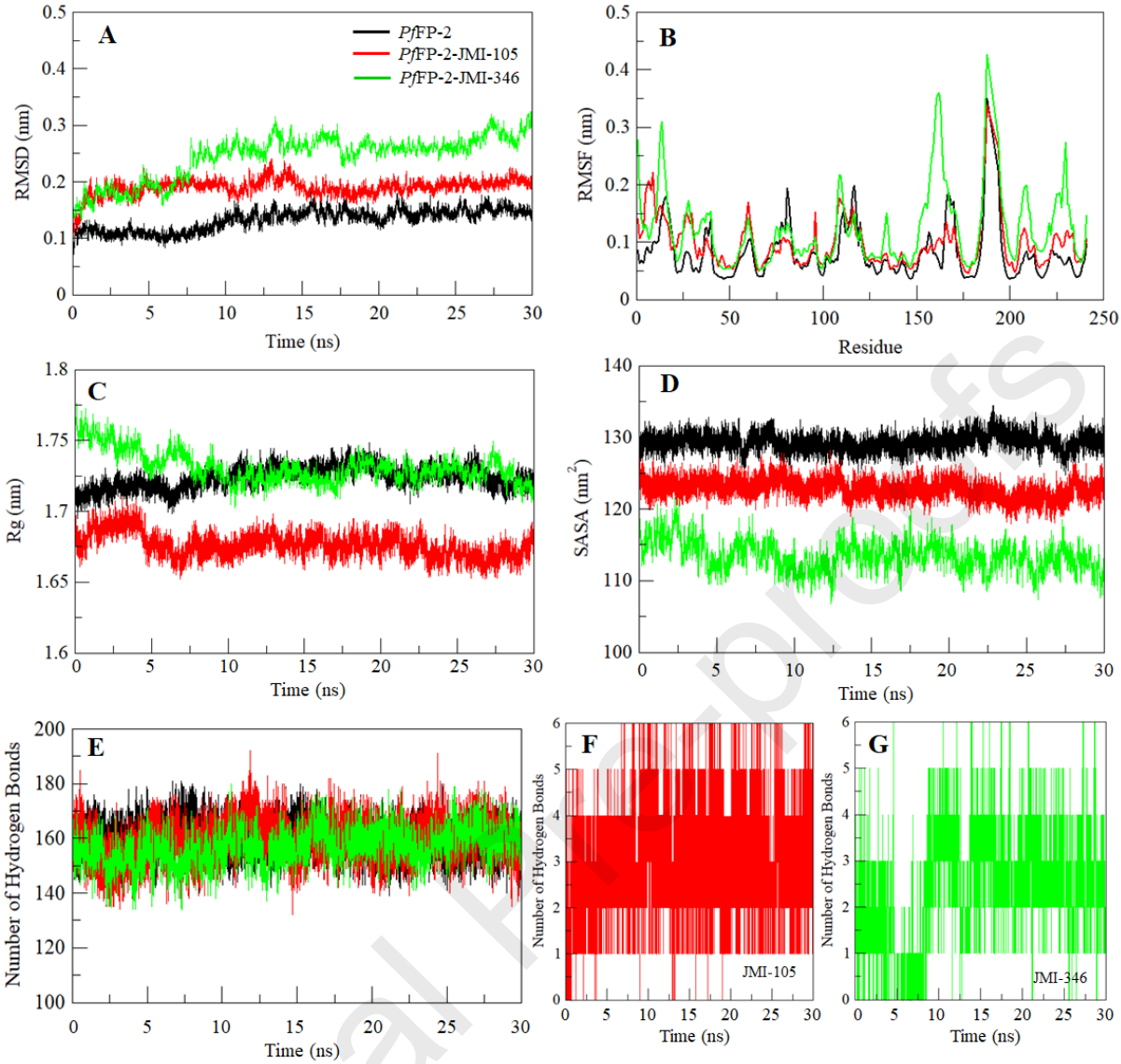


**Figure 2:** Structural dynamics of *Pf*FP-2 upon binding with **JMI-105** and **JMI-346** compounds. (**A**) The RMSD plot of *Pf*FP-2 and its docked complexes (**B**) Residual fluctuations (RMSF) plot of *Pf*FP-2 upon binding with **JMI-105** and **JMI-346** (**C**) Time evolution of radius of gyration ($R_g$) (**D**) SASA plot of *Pf*FP2 as a function of time. The values were obtained from 30 ns MD simulations time scale. Black, red and green represent values obtained for free *Pf*FP-2, *Pf*FP-2-**JMI-105** and *Pf*FP-2-**JMI-346** complex, respectively. (**E**) Time evolution and stability of hydrogen bonds formed intra-protein within *Pf*FP2, and (**F**) Hydrogen bonds formed between **JMI-105** and *Pf*FP2 (**G**) and Hydrogen bonds formed between **JMI-346** and *Pf*FP2. The values were obtained from 30 ns MD simulations time scale. Black, red and green represent values obtained for free *Pf*FP-2, *Pf*FP-2-**JMI-105** and *Pf*FP-2-**JMI-346** complex, respectively.

The dynamics of the secondary structure content in *Pf*FP-2 upon binding with **JMI-105** and **JMI-346** were investigated to assess the changes in *Pf*FP-2. Structural components such as α-helix, β-sheet and turn in *Pf*FP-2 were broken into distinct amino acid residues for each time step, and subsequently, average residues were calculated. The structural elements in free-*Pf*FP-2 remain continual with the least fluctuations, which were equilibrated throughout the entire simulations (**Fig. 3**). The changes in free-*Pf*FP-2 remain continual with fewer fluctuations and equilibrated throughout the simulations (**Fig. 4**). Overall residues participating in secondary structure elements of *Pf*FP-2 upon **JMI-105** and **JMI-346** binding were found to be decreased to some extent due to bend formation in the case of *Pf*FP-2-**JMI-105**, and coil formation in *Pf*FP-2-**JMI-346** complex as compared to free *Pf*FP-2 (**Fig. 4** and **Table 5**). Overall, we did not observe any significant change in the secondary structure content of *Pf*FP-2 upon **JMI-105** and **JMI-346** binding that showed good stability of the complexes.

**Table 5:** Percent residues participating in the secondary structure formation of *Pf*FP2.

| System | Residues participating in the secondary structure formation (%) | | | | | | | |
|---|---|---|---|---|---|---|---|---|
| | Structure* | Coil | β-sheet | β-bridge | Bend | Turn | α-helix | Other# |
| ***Pf*FP2** | 52 | 32 | 18 | 3 | 13 | 11 | 20 | 3 |
| ***Pf*FP-2-JMI-105** | 51 | 31 | 19 | 3 | 15 | 9 | 20 | 3 |
| ***Pf*FP-2-JMI-346** | 49 | 33 | 17 | 2 | 17 | 8 | 22 | 1 |

*Structure = α-helix + β-sheet + β-bridge + Turn; #Other = 5-Helix + 3-Helix

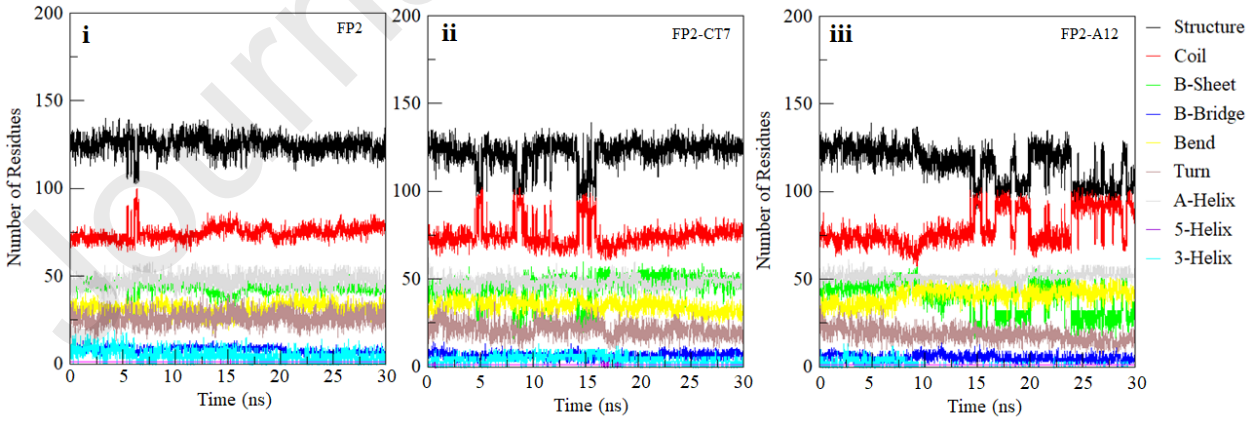


**Figure 3: Secondary structure content** of (**i**) Free *Pf*FP2 and (**ii**) *Pf*FP2 upon JMI-105 binding and (**iii**) *Pf*FP2 upon JMI-346 binding. *Structure = α-helix + β-sheet + β-bridge + Turn.

## *2.2. Chemistry*

Based on the virtual screening of our *in house* library of 652 compounds, **JMI-105** and **JMI-346** were selected (Supplementary data) as mentioned earlier. **JMI-105** is a semi-synthetic triazole derivative of a natural alcohol carvacrol and has been reported previously by our lab [33]. Briefly, carvacrol was propargylated in the presence of propargyl bromide and $K_2CO_3$ to yield alkyne. In another set of reaction, aniline bearing *p*-$OCH_3$ group was converted into corresponding azide. Together, azide & alkyne underwent Cu(I)- catalyzed [3+2] cycloaddition reaction in the presence of $CuSO_4.5H_2O$ in catalytic amount & sodium ascorbate in THF/$H_2O$ (1:2) mixture to yield **JMI-105**. Another compound **JMI-346** is chemically a triazole ester of phenylalanine bearing *p*-methyl substitution on the phenyl ring was also reported previously [34]. Briefly, boc-protected *L*- phenylalanine was coupled with propargyl bromide in the presence of $K_2CO_3$ using DMF as solvent to give alkyne in good yield. In another reaction, diazotization of *p*-toluidine with $NaNO_2$ and concentrated HCl in the presence of $NaN_3$ led to corresponding azide. Later, both alkyne and azide were reacted to obtain the boc-protected triazole derivative via Huisgen 1, 3-diapolar cycloadditon reaction in the presence of $CuSO_4.5H_2O$ and sodium ascorbate in THF: $H_2O$ (1:2) mixture. Finally, deprotection of boc group was carried out using *p*-toulene sulfonic acid (PTSA) in $CH_2Cl_2$ to get **JMI-346**.

## *2.3. Biochemical inhibition of PfFP-2*

### *2.3.1. Enzyme kinetics*

*Plasmodium* cysteine proteases are responsible for different biological progressions. This includes protein trafficking, rupture of membranes, Hb degradation, host cell invasion, and egress from host erythrocytes [12, 53-56]. Among the probable targets for drugs leads falcipain-2 (*Pf*FP-2), known cysteine proteases hydrolyze Hb to provide amino acids for parasite protein synthesis. It is important to find inhibitors of falcipain-2 with suitable properties for novel antimalarial drugs [57-60].

Recombinant *Pf*FP-2 was prepared as described earlier [36]. Enzymatic activity of recombinant *Pf*FP-2 was measured by spectrofluorometry; incubated with substrate Z-Phe-Arg-AMC, a known substrate for cysteine proteases. Cleavage and release of fluorogenic AMC was observed at Em=355 nm and Ex= 460 nm. The result showed the percentage inhibition of *Pf*FP-2 in a dose-determined mode by **JMI-105** and **JMI-346** at different concentrations (1, 5, 7.5, 10, 12.5, 17.5, 20, 22.5 and 25μM) (**Fig. 4A**). The $IC_{50}$ for **JMI-105** and **JMI-346** against recombinant *Pf*FP-2 was found to be 20.56μM and 25.79μM respectively. *Pf*FP-2 was found

to be responsible for cleavage of peptide substrate and release of fluorogenic AMC. Reduction of hydrolysis of Z-Phe-Arg-AMC was observed in **JMI-105** and **JMI-346** samples as compared with untreated samples in a dose dependent manner. Therefore, expansion in percentage inhibition of *Pf*FP-2 with **JMI-105** and **JMI-346** treated samples showed their function to block the *Pf*FP-2.

### *2.3.2. Hemoglobin degradation assay*

Malaria parasites follow proteolytic catabolic pathway for degradation of Hb for their own growth and maturation. Catabolic pathway results in generation of peptides and amino acids in food vacuoles of the parasite [38, 54, 61, 62]. Inhibition of hemoglobinase activity of *Pf*FP-2 by **JMI-105** and **JMI-346** was observed with SDS PAGE and spectrophotometer [36]. **JMI-105** and **JMI-346** at 1, 5, 12.5 and 25µM concentrations were used for incubation with Hb and recombinant *Pf*FP-2 in sodium acetate buffer (pH 5.5) [38]. SDS PAGE analysis confirmed inhibition of degradation of Hb by **JMI-105** at the 12.5µM concentration and **JMI-346** at 25µM concentration (**Fig. 4B**). The percent decrease in Hb hydrolysis was observed by spectrophotometer in dose dependent manner with the treatment of **JMI-105** and **JMI-346** as compared to untreated control confirming that they block the *Pf*FP-2 activity. Use of 12.5 and 25µM concentration of **JMI-105** and **JMI-346**, showed percentage of Hb hydrolysis to be 44.63 ± 5.16% and 34.05 ± 2.63% and 59.88 ± 2.95% and 45.97 ± 4.63% respectively (**Fig. 4C**). Thus, **JMI-105** and **JMI-346** effectively blocks the activity of *Pf*FP-2. However, **JMI-105** was observed to be more effective as compared to **JMI-346** with respect to *Pf*FP-2 inhibition activity.

### *2.3.3. Surface Plasmon Resonance (SPR)*

To confirm the interaction of *Pf*FP-2 with **JMI-105** and **JMI-346**, we studied its strength between the protein-drug using surface plasmon resonance (SPR). Different concentrations of **JMI-105** and **JMI-346** were injected over immobilized recombinant *Pf*FP-2. E-64 was used as positive control. We found that **JMI-105** and **JMI-346** at increasing concentration of 1, 10, 25, 50, 75µM interacted with recombinant *Pf*FP-2. The dissociation equilibration constants (Kd) for the compounds **JMI-105** and **JMI-346** were found to be 56.7µM and 74.0µM indicating direct binding to the recombinant *Pf*FP-2 (**Fig. 4D**).

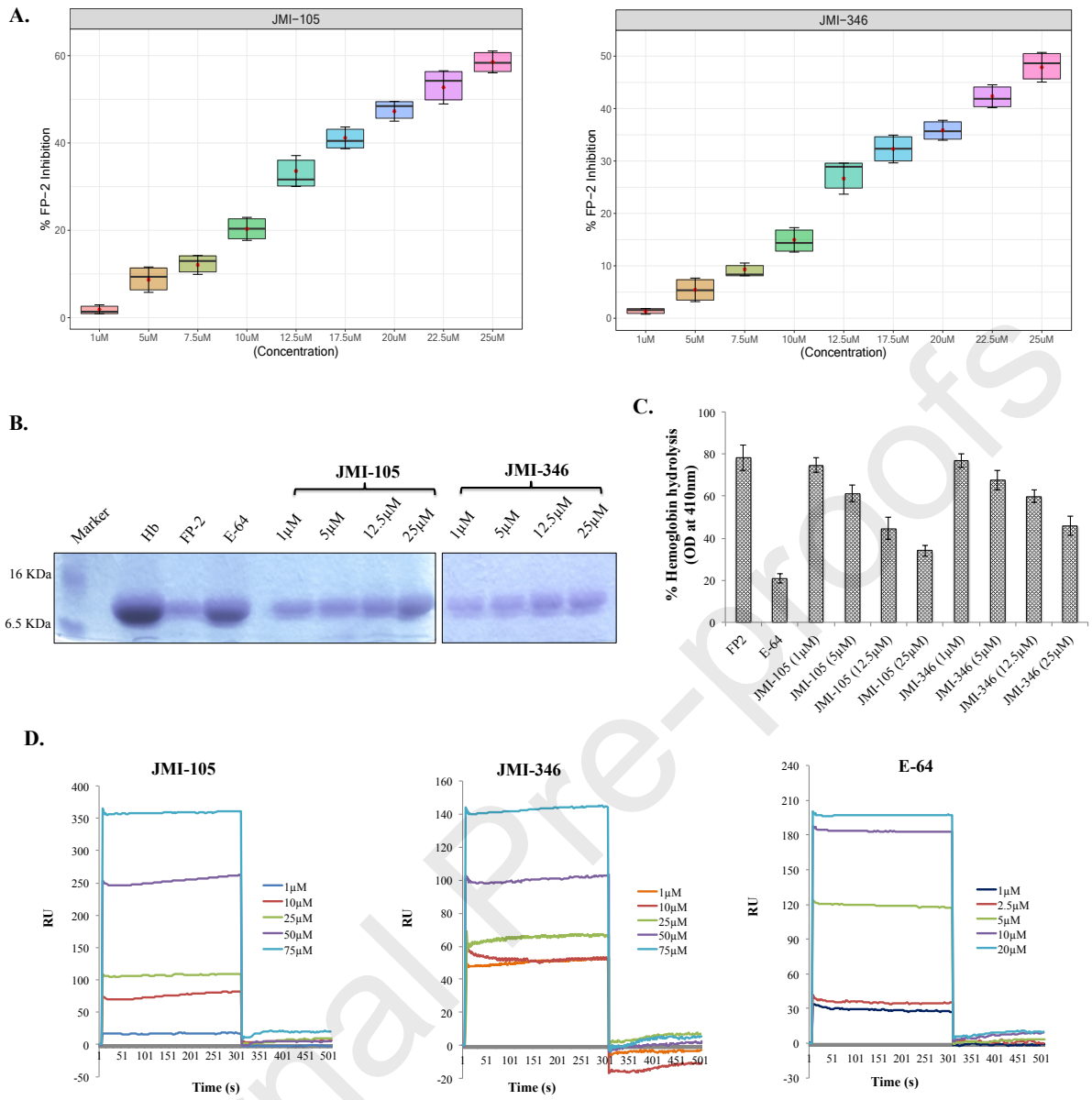


**Figure 4: (A)** Shows *Pf*FP-2 inhibition activity by **JMI-105** and **JMI-346**. Hydrolysis of substrate Z-Phe-Arg-AMC was calculated. Recombinant *Pf*FP-2 was treated with **JMI-105** and **JMI-346** at different concentrations. Z-Phe-Arg-AMC was added to the samples and incubated to obtain fluorescence intensity. The graph showed percentage increase inhibition of *Pf*FP-2, indicating attenuation of hydrolysis of substrate peptide. **(B)** Hemoglobin hydrolysis by *Pf*FP-2 and its inhibition by **JMI-105** and **JMI-346** were checked by SDS PAGE. The dose dependent manner attenuation in hemoglobin hydrolysis was observed in treated samples. **(C)** Inhibition of hemoglobin hydrolysis by **JMI-105** and **JMI-346** was observed using spectrophotometer by taking absorbance at 410 nm. Native Hb was treated with recombinant *Pf*FP-2 and **JMI-105** and **JMI-346** at 1, 5, 12.5, 25µM concentrations. Data was expressed as

mean values ± SD. Experiments were carried out in duplicate. **(D)** shows Surface plasmon resonance analysis. Recombinant *Pf*FP-2 was immobilized on surface of nickel charged NTA SPR chip. Experiment was performed with increasing concentrations of **JMI-105** and **JMI-346** (1, 10, 25, 50, 75µM) at association and dissociation time of 300 and 150 s. E-64 was used as positive control. Hemoglobin degradation activity by *Pf*FP-2 occurs during an early trophozoite stage. *Pf*FP-2 also works beside membrane skeletal ankyrin and protein 4.1 during the late trophozoite and schizont stages of growth of parasite [60, 61].

### *2.3.4. Live-cell imaging*

Live-cell imaging was done to observe the effect of **JMI-105** and **JMI-346** in the intracellular *Pf*FP-2. Parasites from the synchronized trophozoite stage were incubated with **JMI-105** and **JMI-346** to observe the intracellular hydrolysis of substrate Z-Phe-Arg-AMC. *Pf*FP-2 undergoes proteolytic cleavage to the Z-Phe-Arg-AMC products and release fluorogenic AMC as observed with Olympus fluoview 3000 confocal microscope. CellSens analysis software was used to analyse the figures. Around thirty parasites of each sample were monitored but only representative figures are shown here (**Fig. 5A**). Less intensity corresponds to the hindrance of cleavage of peptide substrate Z-Phe-Arg-AMC. **JMI-105** and **JMI-346** treated samples showed attenuation in fluorescence as compared to control untreated sample. Mean gray intensity values of control and **JMI-105** and **JMI-346** treated samples were obtained by spectrofluorometer. The compound treated parasites showed less intensity as compared to untreated control in a dose dependent manner. In untreated sample, the mean intensity was found to be 734.33 ± 133.16 whereas at 20µM concentration of **JMI-105** and **JMI-346,** the mean intensity was 434 ± 86.01 and 517.33 ± 62.40, respectively (**Fig. 5B**). **JMI-105** treated pRBCs showed significant decrease in mean (gray intensity value) as compared to **JMI-346** treated pRBCs and untreated control pRBCs. This represents inhibition effect on *Pf*FP-2 by the hindrance of cleavage of fluorogenic peptide substrate Z-Phe-Arg-AMC [37].

### *2.3.5. Hemozoin Assay*

Hb degradation produces, ferric heme which is a byproduct and proves to be lethal to both the malaria parasites and the host cells [56, 63-65]. Consequently, malaria parasite for its protection resort to crystallization into hemozoin, converting toxic heme into nontoxic metabolites. Hemozoin is a malaria pigment, which is insoluble in water [65, 66]. Spectrophotometric analysis was performed to examine free monomeric heme acquired from

hemozoin. For the quantification of monomeric heme, parasites having ring stage (synchronized) were incubated with **JMI-105** and **JMI-346** and followed up to schizont stage. Parasites treated with **JMI-105** and **JMI-346** showed dose dependent decreased percentage of free monomeric heme as compared to untreated control. At 50µM concentration, **JMI-105** showed 29.7% whereas at **JMI-346** showed 34.7% free heme (**Fig. 5C**). From parasite's hemozoin, free monomeric heme was quantified at 405/750 nm absorbance which later correlated with the reduction in Hb hydrolysis. Crystallization of hemozoin is vital for persistence of malaria parasite that creates an interest towards the development of novel antimalarial drugs [64, 67].

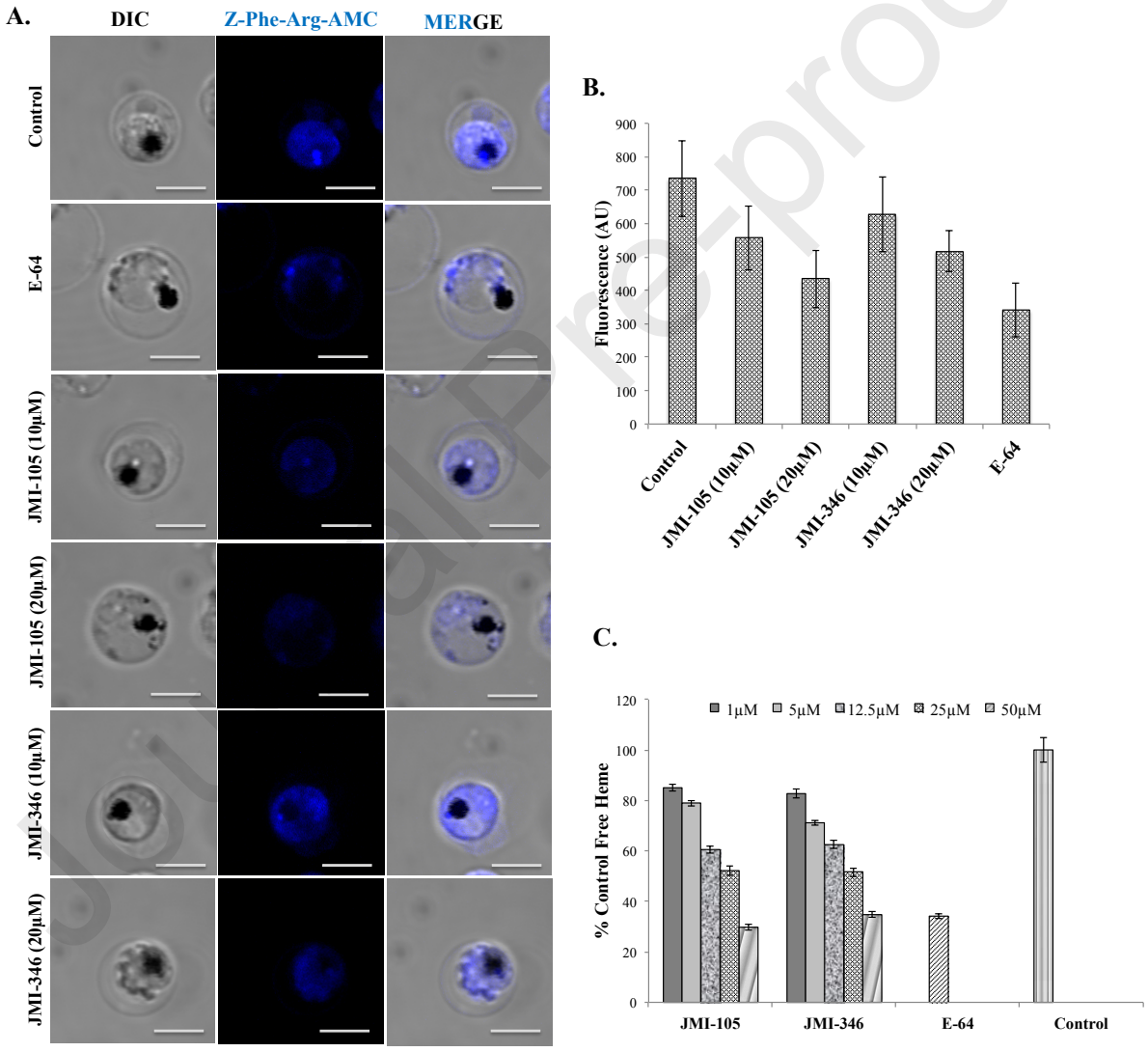


**Figure 5: (A)** Live cell imaging analysis of intracellular hydrolysis of substrate Z-Phe-Arg-AMC showed *Pf*FP-2 inhibitory effect of **JMI-105** and **JMI-346**. Synchronized trophozoites were treated with **JMI-105** and **JMI-346** at 10 and 20µM concentrations. Images showed the

inhibition of *Pf*FP-2 by **JMI-105** and **JMI-346** conferred by the attenuation of proteolytic cleavage of fluorogenic AMC. **(B)** The mean intensity values measured by CellSens analysis software. Parasitized red blood cells (pRBCs) treated with **JMI-105** and **JMI-346;** showed a decrease in mean intensity values of **JMI-105** and **JMI-346** treated pRBCs. **(C)** Graph showed hemozoin inhibition in **JMI-105** and **JMI-346** treated parasites. Synchronized ring-stage parasites exposed to **JMI-105** and **JMI-346** at 1, 5, 12.5, 25 and 50µM concentrations and Percent control free heme was estimated. Experiment was done in triplicate and presented as mean values ± SD, **P < 0.01 *vs*. control: Dunnett's test.

### *2.3.6. Antimalarial activity by SYBR green I based fluorescence assay*

Growth inhibition of **JMI-105** and **JMI-346** on 3D7 *P. falciparum* was observed at different concentrations ranging from 1-100µM. One complete intraerythrocytic growth cycle of *P. falciparum* was examined after the treatment. DNA-specific dye SYBR green I assay and Giemsa staining were performed to observe the growth inhibition. Both **JMI-105** and **JMI-346** were found to be effective against the tested strain and showed inhibitory effects in a concentration dependent manner as compared to untreated control (**Fig. 6A**). Furthermore, **JMI-105** and **JMI-346** were also tested against *Pf*RKL-9 strain. Half-maximal inhibition concentration ($IC_{50}$) of **JMI-105** and **JMI-346** against 3D7 and RKL-9 were calculated (Graph Pad Prism 8 software). $IC_{50}$ values of **JMI-105** and **JMI-346** against 3D7 were found to be 8.8µM and 14.3µM whereas 13µM and 33.8µM were observed against RKL-9 *P. falciparum* strain, respectively. Growth progression analysis was also done with **JMI-105** and **JMI-346** against *P. falciparum* 3D7 strain. Experiment was performed for one complete growth cycle of parasite. Synchronized parasite culture of ring stage was treated with **JMI-105** and **JMI-346** at their $IC_{50}$ concentration. Parasites (no treatment) were taken as control. Thin Giemsa stained blood smears were prepared at different time intervals of 20, 40 and 56-hour post treatment (HPT). Growth progression defect was analyzed by counting ~2000 cells per Giemsa stained slide by light microscope. Morphological analysis was observed in the presence and absence of compounds. It was observed that after 56 HPT, most of the **JMI-105** and **JMI-346** treated parasites were stuck at trophozoite stage showing altered morphology. In untreated control, growth of the cells progressed normally. As compared to untreated control, reduction in percentage of parasitemia was detected. However, in case of **JMI-105,** parasites were found to

be pyknotic whereas in case of **JMI-346** treated parasites, some population of ring-stage parasite was seen indicating delayed progression (**Fig. 6B**).

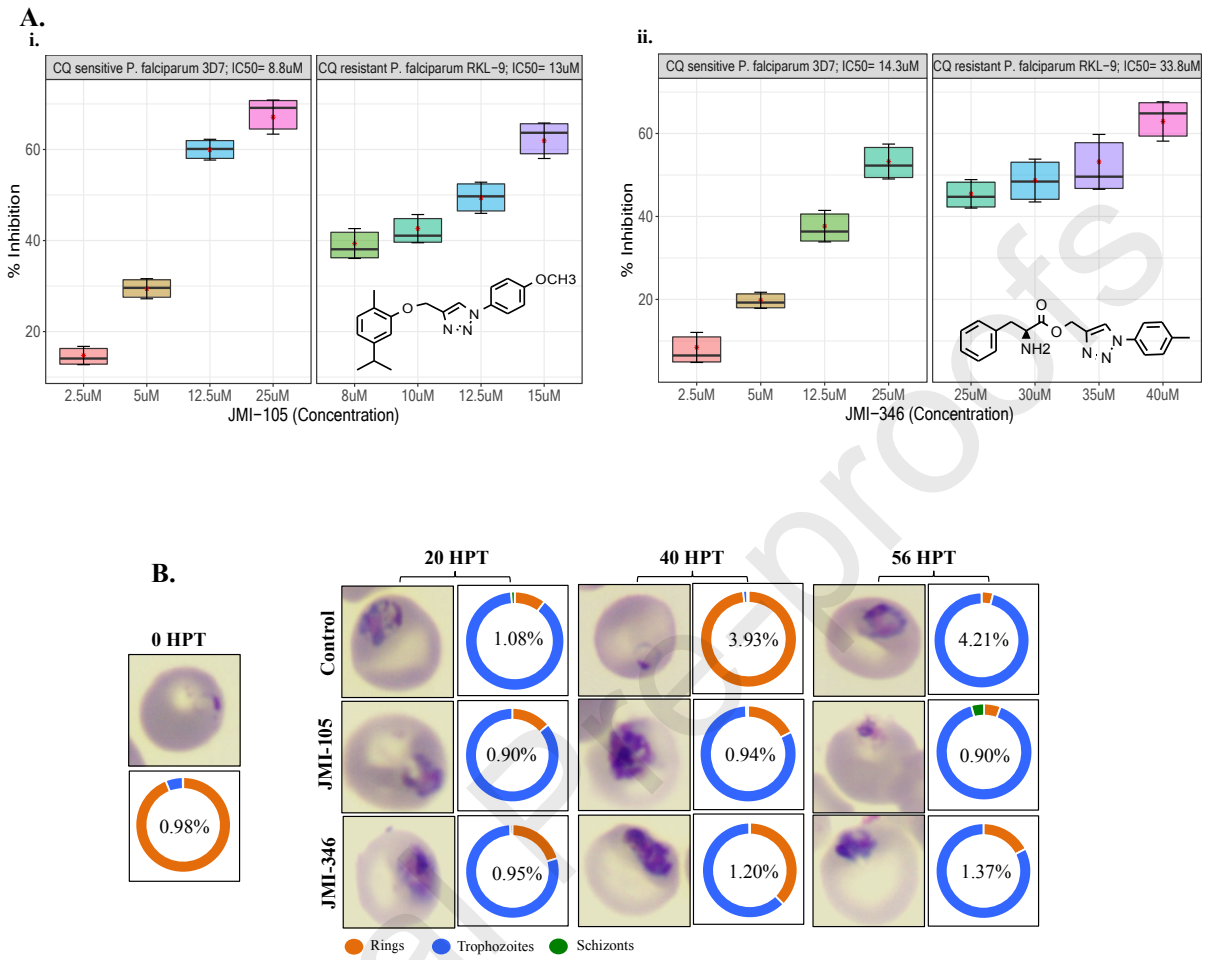


**Figure 6: (A)** *In vitro* growth inhibition of **JMI-105** and **JMI-346** at different concentrations (1-50µM) against 3D7 and RKL-9 strains of *P. falciparum*. Box plot graph shows the antimalarial activity of **JMI-105** and **JMI-346**. Inset of box plot graph show structure of **JMI-105** and **JMI-346** and half-maximal inhibition concentration ($IC_{50}$) of **JMI-105** and **JMI-346** as mentioned against 3D7 and RKL-9 strains of *P. falciparum*. Experiment was performed in triplicate and data was expressed as mean values ± SD. **(B)** Growth progression analysis was done with 3D7 *P. falciparum* after treatment with **JMI-105** and **JMI-346**. Giemsa staining was done to observe morphological changes for one complete growth cycle of parasites at time intervals of 20, 40 and 56 HPT. Figures and pie graphs both showed delayed growth of the parasites.

### *2.3.7. Hemolytic activity*

Spectrophotometric analysis was done to see the effect of **JMI-105** and **JMI-346** on human red blood cells (*h*RBCs) and HEK293 cells. Up to 12.5µM concentration, no significant lysis in RBCs was observed by the **JMI-105** and **JMI-346** whereas 1% Triton-X 100 treated RBCs showed 100% hemolysis (**Fig. 7A**).

### *2.3.8. Cytotoxicity assay*

Compound **JMI-105** and **JMI-346** did not affect the viability of HEK293 cells (**Fig. 7B**) because these compounds are non-cytotoxic to human cells in the concentration range tested.

### *2.3.9. Structure-Activity Relationship (SAR) studies*

The synthetic pathway to achieve SAR derivatives (**5a-5l**) is outlined in (**Scheme 1**). In the reaction sequences, the coupling of (**1**) with propargyl bromide using $K_2CO_3$ in anhyd. DMF gives the corresponding alkyne (**2**) an excellent yield. In another pot, aryl azides (**4a-4l**) were prepared from the substituted anilines (**3a-3l**) by diazotization of aniline with $NaNO_2$ and HCl followed by the reaction with $NaN_3$ all in the single reaction vessel. Finally, both alkyne and azide were subjected to Huisgen 1,3 dipolar cycloaddition reaction in the presence of $CuSO_4.5H_2O$ and sodium ascorbate in THF:$H_2O$ (1:2) mixture. SAR derivatives (**5a-5l**) gave rise moderate to good yields (46-88%). Using FT-IR, $^1$H, $^{13}$C NMR and mass spectrometry, the structures and purity was found to be ≥94% which was confirmed by UPLC. In the IR spectra, the disappearance of the characteristic peak of alkyne C=C and ≡CH stretching and appearance of characteristic peak of =CH (triazole) stretching in the region 3017-3274 cm-$^1$ provided the evidence for the formation of triazole ring. In the $^1$H NMR spectra, appearance of characteristic singlet due to =CH (triazole) in the region 7.69-8.14 ppm confirmed the formation of triazole ring. The methylene (-$CH_2$-) proton linking the natural precursors to the triazole scaffold appeared in the region 5.19-5.33 ppm. In the $^{13}$C NMR spectra, peak at 145.71 and 123.22-124.51 ppm, is due C4 and C5 carbon atoms of the triazole ring. All the protons and carbons appeared at the expected chemical shift values. Mass spectra of all the compounds were found to be in agreement with their molecular formula thus confirming the formation of the desired SAR derivatives. Details of all the spectra are given in the supporting information.

Initial active molecule **JMI-105** [52.73% inhibition of *Pf*FP-2; $IC_{50}$ = 8.8µM (3D7); 13.0 (RKL-9)] as the lead inhibitor in cell-free and cell-based assays was further optimized through SAR. Compounds (**JMI-99** to **JMI-106**) belonging to the series of **JMI-105** were included in

the SAR studies. SAR optimized compounds (**5a-5l**) along with (**JMI-99** to **JMI-106**) were subjected to growth inhibition studies to see their effects on the parasite growth.

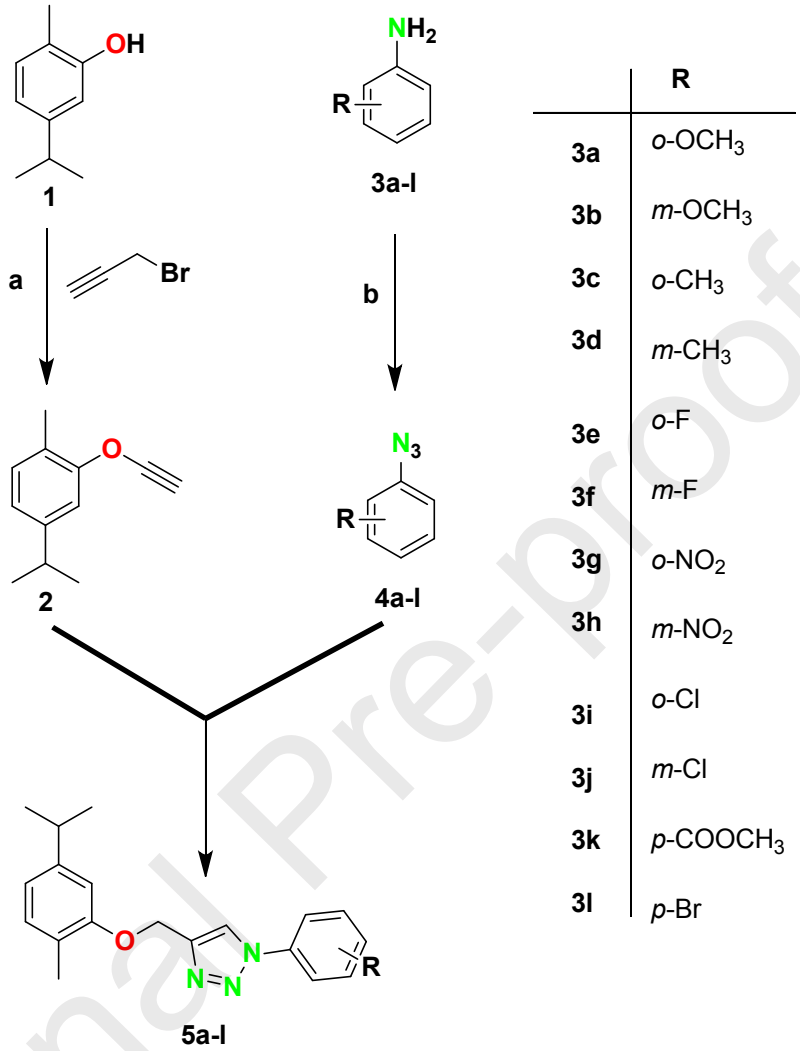


**Scheme 1:** Synthesis of 1,2,3-triazole derivatives, Reagents and conditions: (a) DMF, $K_2CO_3$, 0 °C r.t , 18 h; (b) conc. HCl, $NaNO_2$, $NaN_3$, $H_2O$, EtOAc, 0 °C r.t , 2.5 h ; (c) $CuSO_4.5H_2O$, sodium ascorbate, THF/$H_2O$ (1:2), r.t, 20-24 h.

**JMI-105** showed up to (59.25% inhibition at 10µM) as expected, but unfortunately, none of the SAR derivatives showed significant growth inhibition upto 10µM concentration except **5a** and **5b** (Supplementary data). It was interesting to note that replacement of *p*-$OCH_3$ group as present in **JMI-105** (59.25% inhibition) to *ortho*-position (**5a**, 43% inhibition) or *meta*-position (**5b**, 41% inhibition) at 10µM conc. which gradually diminishes the activity (**Fig. 7C**). To validate our screening strategy, we conducted growth inhibition studies with **JMI-99** to **JMI-106,** which showed maximum of 23% inhibition (**JMI-103**) at 10µM concentration (data given

in supplementary information). This proves that our strategy for the identification of potent and selective *Pf*FP-2 inhibitors is valid and justified. Further, **JMI-105,** which is a semi-synthetic triazole derivative of carvacrol with *p*-$OCH_3$ substitution is indeed a potent anti-malarial compound acting via *Pf*FP-2 inhibition and can be carried forward for further biological evaluation.

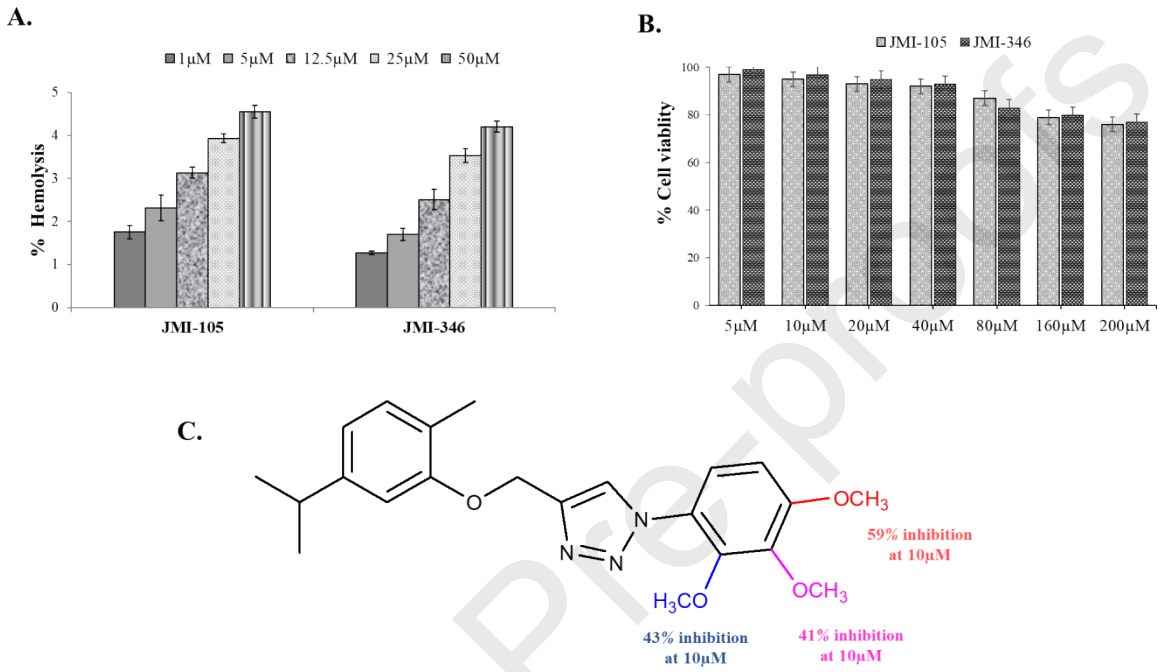


**Figure 7: (A)** Effect of **JMI-105** and **JMI-346** on human RBCs. Different concentrations 1, 5, 12.5, 25, 50µM of **JMI-105** and **JMI-346** were used to treat the RBCs suspension [10% (v/v)] and incubated for 1h. Non-significant effect was observed in the treated samples upto 25µM concentration. **(B)** Colorimetric MTT assay was used to observe the cytotoxicity of **JMI-105** and **JMI-346** against human embryonic kidney (HEK293) cells at 5-200µM concentrations. The graph showed percent cell viability of HEK293 and the experiment was performed in triplicate. Data was expressed as mean values ± SD. **(C)** Replacement of -$OCH_3$ group from *para* position (**JMI-105**) to *ortho* (**5a**) or *meta* (**5b**) position led to the decrease in the inhibition of the malaria parasite.

### *2.3.10. In vivo antimalarial activity*

*In vivo* antimalarial efficacy of **JMI-105** was examined in *P. berghei* ANKA infected BALB/c mice model. Infected mice were administered intraperitoneally with **JMI-105** at 30 and 100mg/Kg doses. Thin blood smears were made from *P. berghei* infected mice to check the

parasitemia for upto eight consecutive days [68]. Significant reduction in the percentage parasitemia and mortality rate was observed in **JMI-105** treated group of mice as compared to untreated control group on day 8 post infection. Percentage parasitemia of **JMI-105** treated group was observed to be 14.67% and 11.21% in 30 and 100mg/Kg as compared to the untreated control wherein percent parasitemia was 43.34% on day 8 (**Fig. 8Ai**). Survival of group of mice was observed upto 18 days post infection. Mean survival time (MST) showed improvement in mortality rate in case of **JMI-105** 30mg/Kg (MST= 9.26 days) and 100mg/Kg (MST= 10.72 days) as compared to control (MST=7 days). Graph was plotted as percentage mean survival time (**Fig. 8ii**). The decrease in parasite load was found to be more effective in case of **JMI-105** 100mg/Kg as compared to 30mg/Kg dose concentration for eight consecutive days post infection.

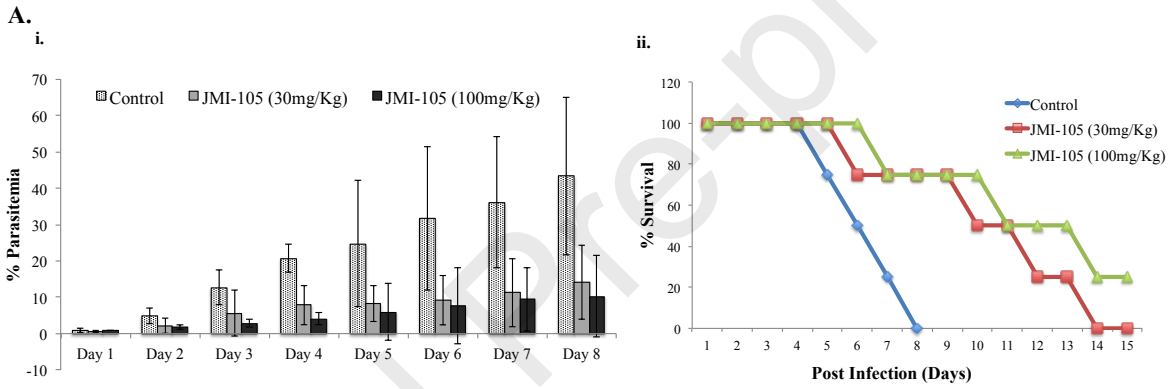


**Figure 8: (A)** Evaluation of *in vivo* antimalarial activity **of JMI-105** on *P. berghei* ANKA infected Balb/c mice. **JMI-105** (30 mg/Kg and 100 mg/Kg body weight; n=4) was administered intra-peritoneally in *P. berghei* ANKA infected Balb/c mice for eight consecutive days. Untreated group of mice were taken as control. Thin blood smears were made upto day 8 post infection. **(Ai)** Graph showed percentage increase in parasitemia; **(Aii)** Survival of mice was observed up to 18 days post infection. Graph showed percentage survival of mice.

## 3. Materials and Methods

Through the combination of various bioinformatic techniques such as filtering tools, AutoDock Vina, PyMOL, Discovery Studio Visualizer and *in vitro*, *in vivo* biological evaluation of the hit compounds as well as their SAR derivatives, this study paved the way to develop semi-synthetic derivative of carvacrol (**JMI-105**) as a potential *Pf*FP-2 inhibitor with appreciable *in vitro* and *in vivo* antimalarial efficacy.

### *3.1. In silico studies*

#### *3.1.1 Drug-likeness assessment of In-house library*

Initially, an *in-house* library of 652 compounds was filtered out based on their drug-like properties using the DruLiTo tool which is an open-source software developed by NIPER http://www.niper.gov.in/pi_dev_tools/DruLiToWeb/DruLiTo_index.html [29]. This consists of various drug-likeness filters based on Lipinski's rule, Veber rule, Ghose rule, CMC-50, Quantitative Estimate of Drug-likeness (QED) properties, etc. We applied all these filters with default parameters to obtain those compounds which show resemblance to drug molecules. Further, the selected compounds were filtered out based on their ADMET properties using SwissADME webserver. These compounds were also checked for any PAINS and carcinogenic pattern to select safer compounds. The PAINS filter was applied to sidestep those compounds possessing PAINS patterns thus may have a higher tendency of binding towards multiple targets [2].

#### *3.1.2 Pre-processing of FP-2 structure and compounds*

The three-dimensional coordinates of *Pf*FP-2 and *Pf*FP-3 crystal structures were taken from the Protein Data Bank (PDB ID: 3BPF and 3BPM, respectively), and all the bound crystallized water molecules and co-crystallized ligands were deleted from the original structures [30]. The structures were remodeled while using MODELLER 9.21 to fill-up the break due to some missing residues. The final structures were prepared using MGL tools for screening. An *in-house* library of compounds was used to process three-dimensional status. Compounds were converted into PDBQT file format using the Open Babel module of PyRx to perform structure-based virtual screening. All the selected compound structures were drawn in ChemDraw and processed in MGL tools [31].

#### *3.1.3 Molecular docking*

We have performed the structure-based molecular docking to further screen the compounds on the basis of their binding affinity towards *Pf*FP-2 and *Pf*FP-3. This screening was performed while using AutoDock Vina to find out compounds based on their affinity and interaction with *Pf*FP-2 and *Pf*FP-3. The docking was structurally blind for all the compounds with exhaustiveness 8 where they were free to move and search their preferential binding sites in

the proteins. AutoDock Vina was used for docking purpose to generate the detailed ligand-receptor interactions. PyMOL [30] and Discovery Studio were used in visualization procedure to analyze the bound conformation stabilized by various interactions between the selected compounds and the protein.

### *3.1.4 MD simulations*

All-atoms MD simulations studies were performed on DELL® server with Intel® Xeon® CPU E5-2609 v3 @ 1.90 GHz processor. MD simulation was performed on free FP-2 and in-presence of JMI-105 and JMI-346 at 300 K of molecular mechanics level for 30 ns. The GROMOS96 43a1 force-field was utilized in GROMACS 5.1.2 to perform simulations. The ligands topologies were generated from the PRODRG server and merged into the parent coordinates of FP-2 for systems preparation. A cubic box of 10 Å dimension was used for solvating the systems in the SPC216 model using *gmx solvate* module. A run of 1500 steps of steepest descent was carried out for energy minimization [27]. The final MD run was set to 30,000 ps for all three systems, and the generated trajectories were examined while utilizing the inbuilt GROMACS utilities and visualized in VMD and QtGrace tools as described in our earlier communication [32].

### *3.2 Chemical synthesis*

All the required chemicals were purchased from Merck, Sigma-Aldrich and were used without further purification. TLC was performed using precoated Merck Silica gel 60 $F_{254}$ TLC aluminium sheets and UV light (254 nm) $I_2$ vapor staining was used for visualization of spots. Column chromatography was performed with Merck 230-400 mesh silica gel. Digital Buchi melting point apparatus (M-560) was used for measurement of melting points. IR spectra were recorded and only major peaks are reported in $cm^{-1}$ by Agilent Cary 630 FT-IR spectrometer. $CDCl_3$ (as solvent) with TMS as an internal standard on Bruker Spectrospin DPX-300 spectrometer at 300 MHz and 75 MHz were used for $^1H$ and $^{13}C$ NMR spectra. s (singlet), d (doublet), t (triplet), m (multiplet) or brs (broad) were labelled as splitting pattern. The chemical shift values of $^1H$ NMR were reported in parts per million (ppm) relative to residual solvent ($CDCl_3$, $\delta$ 7.26) and $^{13}C$ NMR chemical shifts ($\delta$) of $^{13}C$ NMR were reported in ppm relative to ($CDCl_3$, $\delta$ 77.16) and Hertz (Hz) is the unit of coupling constants ($J$). Agilent Quadrupole-6150 LC/MS spectrometer was used for recording of mass spectra. Chemical synthesis and

spectral characterization of **JMI-105** [33] and **JMI-346** [34] was reported earlier. Synthesis protocols and spectral characterization of SAR derivatives (**5a-5l**) is discussed below:

### *3.2.1 General procedure for the synthesis of alkyne (2)*

Briefly, the natural alcohol carvacrol (**1)** (1.0 mM) was dissolved in anhyd. DMF and 2.0 mmol of potassium carbonate was added and allowed to stir for 15 min at 0° to rt. 1.2 mM of propargyl bromide was added to reaction flask and stirred for overnight. Upon completion of the reaction as evident by TLC, addition of water to quenched the reaction and extracted with ethyl acetate (30 mL×2). The organic layer was washed with brine, dried over anhyd. sodium sulphate and concentrated under *vacuo*. Crude obtained was purified by column chromatography (CC) by use of ethyl acetate:hexane (3:7) to get the pure alkyne product [33].

### *3.2.2 General procedure for the synthesis of azides (4a-l)*

To the solution of substituted aniline **(3a-l)** (3.22 mmol) in ethyl acetate (6 mL) kept at 0 °C was added conc. HCl (1.29 mL) followed by addition of a solution of $NaNO_2$ (3.87 mmol) in water (4.03 mL) with constant stirring. After stirring for 1 h at 0 °C, solution of $NaN_3$ (3.87 mmol) in water (4.03 mL) was added to the mixture and allowed to stir at rt till the reaction completes. Reaction mixture was poured in water and extracted with ethyl acetate then dried over anhyd. $Na_2SO_4$. Further, concentrated under *vacuo* to give azide which was used without purification [33].

### *3.2.3 Synthesis of 1,2,3-triazole derivatives of carvacrol (5a-5l)*

Finally, a solution of azide (**3a-l**) (1.06 mmol) and alkyne (**2**) (1.06 mmol) in THF/$H_2O$ (1:2, 9 ml) was added to sodium ascorbate (0.55 mmol) and $CuSO_4.5H_2O$ (0.18 mmol) and stirred overnight at rt. The obtained solid was filtered and washed with water then purified by CC using a solution of ethyl acetate:hexane (1:9) to yield pure triazole derivatives of carvacrol [35].

#### *3.2.3.1 4-((5-isopropyl-2-methylphenoxy)methyl)-1-(2-methoxyphenyl)-1H-1,2,3-triazole* **(5a):**

Light cream liquid, yield: 63%, $R_f$ = 0.65 (ethyl acetate:hexane = 30:70); $^1$H NMR (300 MHz, $CDCl_3$) (δ, ppm): 8.14 (s, 1H, triazole), 7.80 (d, J = 7.5 Hz, 1H, Ar-H), 7.42 (d, J = 7.5 Hz, 1H,

Ar-H), 7.09 (d, J = 7.2 Hz, 1H, Ar-H),7.09 (d, J = 7.2 Hz, 1H, Ar-H), 7.07 (t, J = 7.2 Hz, 1H, Ar-H), 6.89 (s, 1H, Ar-H), 6.77 (d, J = 7.2 Hz, 1H, Ar-H), 5.32 (s, 2H, $CH_2$), 3.87( s, 3H, $OCH_3$), 2.93-2.84 (m, 1H, CH), 2.21 (s, 3H, $CH_3$), 1.25(d, J = 6.6 Hz, 6H, isopropyl); $^{13}C$ NMR (75 MHz, $CDCl_3$) (δ, ppm): 156.46, 151.17, 148.04, 144.21, 130.56, 126.33, 124.74, 121,24, 118.73, 112.26, 110.28, 77.46, 77.04, 76.89, 76.61, 62.51, 55.96, 34.10, 24.13, 15.91; ESI-MS (m/z) calcd. for $C_{20}H_{23}N_3O_2$: 337.18; Found: 338.13 $[M+H]^+$; IR (neat): ν ($cm^{-1}$) 3017 (=CH str., triazole).

*3.2.3.2 4-((5-isopropyl-2-methylphenoxy)methyl)-1-(3-methoxyphenyl)-1H-1,2,3-triazole* **(5b):**

White powder, yield: 69%, mp: 66.2 °C, $R_f$ = 0.82 (ethyl acetate:hexane = 30:70); $^1H$ NMR (300 MHz, $CDCl_3$) (δ, ppm): 8.01 (s, 1H, triazole), 7.41 (t, J = 8.1 Hz, 1H, Ar-H), 7.34 (s, 1H, Ar-H), 7.26 (d, J = 6.9 Hz, 1H, Ar-H), 7.08 (d, J = 7.5 Hz, 1H, Ar-H), 6.96 (d, J = 7.5 Hz, 1H, Ar-H),6.79 (s,1H, Ar-H), 6.78 (d, J = 6.6 Hz, 1H, Ar-H), 5.31 (s, 2H, $CH_2$), 3.88( s, 3H, $OCH_3$), 2.92-2.83 (m, 1H, CH), 2.22 (s, 3H, $CH_3$), 1.24(d, J = 6.6 Hz, 6H, isopropyl);. $^{13}C$ NMR (75 MHz, $CDCl_3$) (δ, ppm): 160.62, 156.30, 148.11, 145.60, 130.65, 130.54, 124.27, 114.70, 110.12, 106.46, 77.59, 77.47, 77.04, 76.74, 76.62, 62.35, 55.65, 34.09, 24.12, 15.92; ESI-MS (m/z) calcd. for $C_{20}H_{23}N_3O_2$: 337.18; Found: 338.28 $[M+H]^+$; IR (neat): ν ($cm^{-1}$) 3147 (=CH str., triazole).

*3.2.3.3 4-((5-isopropyl-2-methylphenoxy)methyl)methyl)-1-o-tolyl-1H-1,2,3-triazole* **(5c):**

Light yellow liquid, yield: 84%, $R_f$= 0.65 (ethyl acetate:hexane = 30:70); $^1H$ NMR (300 MHz, $CDCl_3$) (δ, ppm): 7.69 (s, 1H, triazole), 7.28 (d, J = 8.4 Hz, 2H, Ar-H), 6.99 (d, J = 7.5 Hz, 2H, Ar-H), 6.79 (s, 1H, Ar-H), 6.71 (t, J = 7.8 Hz, 2H, Ar-H), 5.27 (s, 2H, $CH_2$), 2.82-2.78 (m, 1H, CH), 2.17 (s, 3H, $CH_3$), 2.13( S, 3H, $CH_3$), 1.16 (d, J = 6.6 Hz, 6H, isopropyl); $^{13}C$ NMR (75 MHz, $CDCl_3$) (δ, ppm): 156.30, 147.82, 144.86, 133.75, 131.50, 130.64, 129.95, 119.09, 118.88, 110.25, 77.47, 76.62, 75.14, 62.53, 56.00, 34.10, 29.72, 24.08, 17.85, 15.81; ESI-MS (m/z) calcd. for $C_{20}H_{23}N_3O$: 321.18; Found: 320.28 $[M-H]^-$; IR (neat): ν ($cm^{-1}$) 3274(=CH str., triazole).

*3.2.3.4 4-((5-isopropyl-2-methylphenoxy)methyl)-1-m-totlyl-1H-1,2,3-triazole* **(5d):**

Light orange powder, yield: 46%, $R_f$ = 0.68 (ethyl acetate:hexane = 30:70); $^1$H NMR (300 MHz, $CDCl_3$) (δ, ppm): 7.93 (s, 1H, triazole), 7.50 (s, 1H, Ar-H), 7.31 (t, J = 7.8 Hz, 1H, Ar-H), 7.17 (d, J = 7.8 Hz, 1H, Ar-H), 7.00 (d, J = 7.2 Hz, 1H, Ar-H),6.70 (d, J = 7.5 Hz, 1H, Ar-H),6.79 (s,1H, Ar-H), 6.60 (d, J = 7.8 Hz, 1H, Ar-H), 5.27 (s, 2H, $CH_2$), 2.82-2.80 (m, 1H, CH), 2.42 (s, 3H, $CH_3$), 1.17(d, J = 4.8 Hz, 6H, isopropyl); $^{13}$C NMR (75 MHz, $CDCl_3$) (δ, ppm): 156.32, 148.12, 145.55, 140.04, 130.64, 129.61, 124.267, 121.31, 120.65, 118.82, 117.70, 110.10, 77.47, 76.62, 62.37, 34.10, 29.72, 24.13, 15.95, 1.041; ESI-MS (m/z) calcd. for $C_{20}H_{23}N_3O$: 321.18; Found: 322.30 $[M+H]^+$; IR (neat): ν ($cm^{-1}$) 3064(=CH str., triazole).

*3.2.3.5 1-(2-fluorophenyl)-4-((5-isopropyl-2-methylphenoxy)methyl)-1H-1,2,3-triazole* **(5e):**

Off white powder, yield: 79%, mp:62.3°C, $R_f$ = 0.63 (ethyl acetate:hexane = 30:70); $^1$H NMR (300 MHz, $CDCl_3$) (δ, ppm): 8.14 (s, 1H, triazole), 7.97 (t, J = 9.8 Hz, 1H, Ar-H), 7.44 (d, J = 7.5 Hz, 1H, Ar-H), 7.33 (t, J = 7.8 Hz, 1H, Ar-H), 7.07 (d, J = 7.5 Hz, 1H, Ar-H), 7.25 (s, 1H, Ar-H), 6.78 (d, J = 7.5 Hz, 1H, Ar-H), 5.33 (s, 2H, $CH_2$), 2.91-2.86 (m, 1H, CH), 2.21 (s, 3H, $CH_3$), 1.25 (d, J = 6.6 Hz, 6H, isopropyl). $^{13}$C NMR (75 MHz, $CDCl_3$) (δ, ppm): 156.31, 151.72, 148.07, 145.31, 130.64, 130.24 (d, *J* = 7.72 Hz), 125.29, 125.24, 124.35, 123.76 (d, *J* = 8.025 Hz), 118.87, 117.18, 116.91, 110.16, 77.46, 76.61, 62.28, 34.10, 24.11, 15.88; ESI-MS (m/z) calcd. for $C_{19}H_{20}FN_3O$: 325.16; Found: 326.28 $[M+H]^+$; IR (neat): ν ($cm^{-1}$) 3132 (=CH str., triazole).

*3.2.3.6 1-(3-fluorophenyl)-4-((5-isopropyl-2-methylphenoxy)methyl)-1H-1,2,3-triazole* **(5f):**

White powder, yield: 80%, mp:100.1 °C, $R_f$ = 0.68 (ethyl acetate:hexane = 30:70); $^1$H NMR (300 MHz, $CDCl_3$) (δ, ppm): 8.03 (s, 1H, triazole), 7.64 (d, J = 5.4 Hz, 2H, Ar-H), 7.46 (s, 1H, Ar-H), 7.16 (d, J = 7.2 Hz, 1H, Ar-H), 7.10 (t, J = 7.5 Hz, 1H, Ar-H), 6.86(s,1H, Ar-H), 6.78 (d, J = 7.5 Hz, 1H, Ar-H), 5.31 (s, 2H, $CH_2$), 2.93-2.83 (m, 1H, CH), 2.22 (s, 3H, $CH_3$), 1.24(d, J = 6.9 Hz, 6H, isopropyl); $^{13}$C NMR (75 MHz, $CDCl_3$) (δ, ppm): 164.75, 161.45, 156.23, 148.14, 145.98, 138.24, 131.23 (d, *J* = 8.85 Hz), 130.69, 124.25, 120.48, 118.93, 115.75 (d, *J* = 21.75 Hz), 110.07, 108.36 (d, *J* = 25.8 Hz), 77.47, 76.62, 62.28, 34.10, 15.93, ESI-MS (m/z) calcd. for $C_{19}H_{20}FN_3O$: 325.16; Found: 326.11 $[M+H]^+$; IR (neat): ν ($cm^{-1}$) 3131(=CH str., triazole).

*3.2.3.7 4-((5-isopropyl-2-methyphenoxy)methyl)-1-(2-nitrophenyl)-1H-1,2,3-triazole* **(5g):**

Dark yellow liquid, yield: 88%, $R_f$ = 0.33 (ethyl acetate:hexane = 30:70); $^1$H NMR (300 MHz, $CDCl_3$) (δ, ppm): 7.90 (s, 1H, triazole), 8.10 (d, J = 7.8 Hz, 1H, Ar-H), 7.69 (t, J = 7.5 Hz, 1H, Ar-H), 7.66 (d, J = 7.2 Hz, 1H, Ar-H), 7.63 (t, J = 6.3 Hz, 1H, Ar-H), 7.07 (d, J = 7.5 Hz, 1H, Ar-H), ), 6.86 (s, 1H, Ar-H), 6.78 (d,1H, J=7.5Hz, Ar-H), 5.19 (s, 2H, $CH_2$), 2.93-2.84 (m, 1H, CH), 2.25 (s, 3H, $CH_3$), 1.24 (d, J = 6.9 Hz, 6H, isopropyl); $^{13}$C NMR (75 MHz, $CDCl_3$) (δ, ppm): 156.23, 148.17, 145.66, 144.53, 133.82, 130.83, 127.99, 125.60, 124.28, 123.97, 118.96, 110.18, 77.45, 77.03, 76.61, 62.32, 34.09, 24.11, 15.89; ESI-MS (m/z) calcd. for $C_{19}H_{20}N_4O_3$: 352.15; Found: 353.28 $[M+H]^+$; IR (neat): ν ($cm^{-1}$) 3144 (=CH str., triazole).

*3.2.3.8 4-((5-isopropyl-2-methyphenoxy)methyl)-1-(3-nitrophenyl)-1H-1,2,3-triazole* **(5h):**

Light yellow powder, yield: 83%, mp:122.8 °C, $R_f$ = 0.52 (ethyl acetate:hexane = 30:70); $^1$H NMR (300 MHz, CDCl3) (δ, ppm): 8.63 (s, 1H, triazole), 8.31 (d, J = 8.1 Hz, 1H, Ar-H), 8.15 (s, 1H, Ar-H), 8.20 (d, J = 8.1 Hz, 1H, Ar-H), 7.76 (t, J = 8.1 Hz, 1H, Ar-H), 7.09 (d, J = 7.8 Hz, 1H, Ar-H), 6.81(s,1H, Ar-H), 6.79 (d, J = 7.8 Hz, 1H, Ar-H), 5.34 (s, 2H, $CH_2$), 2.91-2.84 (m, 1H, CH), 2.24 (s, 3H, $CH_3$), 1.25(d, J = 6.9 Hz, 6H, isopropyl); $^{13}$C NMR (75 MHz, $CDCl_3$) (δ, ppm): 156.14, 148.96,146.57, 137.74, 131.01, 130.74, 126.00, 124.25, 123.27, 120.42, 119.03, 115.33, 110.02, 77.45, 76.60, 62.18, 34.09, 24.11, 15.94; ESI-MS (m/z) calcd. for $C_{19}H_{20}N_4O_3$: 352.15; Found: 353.28 $[M+H]^+$; IR (neat): ν ($cm^{-1}$) 3132(=CH str., triazole).

*3.2.3.9 1-(2-chlorophenyl)-4-((5-isopropyl-2-methyphenoxy)methyl)-1H-1,2,3-triazole* **(5i):**

Dark yellow liquid, yield: 66%, $R_f$ = 0.61 (ethyl acetate:hexane = 30:70); $^1$H NMR (300 MHz, $CDCl_3$) (δ, ppm): 8.02 (s, 1H, triazole), 7.64 (t, J = 7.2 Hz, 1H, Ar-H), 7.58 (t, J = 7.2 Hz, 1H, Ar-H), 7.07 (d, J = 7.8 Hz, 1H, Ar-H), 6.87 (s, 1H, Ar-H), 6.78 (d,1H, J=7.8Hz, Ar-H), 5.34 (s, 2H, $CH_2$), 2.90-2.86 (m, 1H, CH), 2.21 (s, 3H, $CH_3$), 1.24 (d, J = 6.9 Hz, 6H, isopropyl); $^{13}$C NMR (75 MHz, $CDCl_3$) (δ, ppm): 156.31, 148.09, 144.77, 144.53, 134.92, 130.80, 128.68, 127.94, 127.82, 124.52, 124.39, 118.89, 110.24, 77.47, 76.62, 62.43, 34.10, 24.13, 15.90; ESI-MS (m/z) calcd. for $C_{19}H_{20}ClN_3O$: 341.13; Found: 342.10 $[M+H]^+$, 344.09 $[M+H+2]^+$; IR (neat): ν ($cm^{-1}$) 3144 (=CH str., triazole).

*3.2.3.10 1-(3-chlorophenyl)-4-((5-isopropyl-2-methyphenoxy)methyl)-1H-1,2,3-triazole* **(5j):**

White powder, yield: 80%, mp:93.9 °C, $R_f$ = 0.71 (ethyl acetate:hexane = 30:70); $^1$H NMR (300 MHz, $CDCl_3$) (δ, ppm): 8.02 (s, 1H, triazole), 7.80 (s, 1H, Ar-H), 7.65 (d, J = 7.8 Hz, 1H,

Ar-H), 7.47 (t, J = 8.1 Hz, 1H, Ar-H), 7.44 (d, J = 8.1 Hz, 1H, Ar-H), 7.08 (d, J = 7.5 Hz, 1H, Ar-H), 6.86(s,1H, Ar-H), 6.79 (d, , J = 6.6 Hz, 1H, Ar-H), 5.31 (s, 2H, $CH_2$), 2.93-2.83 (m, 1H, CH), 2.22 (s, 3H, $CH_3$), 1.24(d, J = 6.9 Hz, 6H, isopropyl); $^{13}C$ NMR (75 MHz, $CDCl_3$) (δ, ppm): 156.23, 148.14, 146.01, 137.87, 135.62, 130.85, 128.89, 124.25,120.85, 120.45, 118.93, 118.55, 110.07, 77.46, 77.03,62.29, 34.09, 24.12, 15.93, ESI-MS (m/z) calcd. for $C_{19}H_{20}ClN_3O$: 341.13; Found: 342.10 $[M+H]^+$, 344.08 $[M+H+2]^+$; IR (neat): ν ($cm^{-1}$) 3144(=CH str., triazole).

*3.2.3.11 Methyl4-(4-((5-isopropyl-2-methyphenoxy)methyl)-1H-1,2,3-triazole-1-yl)benzoate* **(5k):**

yellow powder, yield: 71%, mp:106.1 °C, $R_f$ = 0.57 (ethyl acetate: hexane = 30:70); $^1H$ NMR (300 MHz, $CDCl_3$) (δ, ppm): 8.10 (s, 1H, triazole), 8.21 (d, J = 8.7 Hz, 2H, Ar-H), 7.86 (d, J = 8.4 Hz, 2H, Ar-H), 7.08 (d, J = 7.8 Hz, 1H, Ar-H), 6.87 (s, 1H, Ar-H), 6.79 (d, J = 7.5 Hz, 1H, Ar-H), 6.79 (d, , J = 7.5 Hz, 1H, Ar-H), 5.32 (s, 2H, $CH_2$), 2.93-2.83 (m, 1H, CH), 2.23 (s, 3H, $CH_3$), 1.24(d, J = 6.9 Hz, 6H, isopropyl); $^{13}C$ NMR (75 MHz, $CDCl_3$) (δ, ppm): 165.74, 156.22, 148.14, 146.14, 140.07, 131.36, 130.69, 124.24, 120.37, 119.96, 118.95, 110.08, 77.46,77.03, 76.61, 62.27, 52.45, 34.09, 29.70, 24.10, 15.91; ESI-MS (m/z) calcd. for $C_{21}H_{23}N_3O_3$: 365.17; Found: 366.16 $[M+H]^+$; IR (neat): ν ($cm^{-1}$) 3134 (=CH str., triazole).

*3.2.3.12 1-(4-bromophenyl)-4-((5-isopropyl-2-methyphenoxy)methyl)-1H-1,2,3-triazole* **(5l):**

yellow powder, yield: 71%, mp:106.1 °C, $R_f$ = 0.57 (ethyl acetate:hexane = 30:70); $^1H$ NMR (300 MHz, $CDCl_3$) (δ, ppm): 8.12 (s, 1H, triazole), 7.64 (s, 1H, Ar-H), 7.08 (d, J = 7.8 Hz, 1H, Ar-H), 6.78 (d, J = 7.2 Hz, 1H, Ar-H), 5.31 (s, 2H, $CH_2$), 2.92-2.83 (m, 1H, CH), 2.22(s, 3H, $CH_3$), 1.24(d, J = 6.9 Hz, 6H, isopropyl); $^{13}C$ NMR (75 MHz, $CDCl_3$) (δ, ppm): 156.24, 148.14, 145.99, 136.00, 132.93, 130.68, 124.23,122.49,121.98, 120.39, 118.92, 110.07, 77.46,77.04, 76.62, 62.29, 52.45, 34.09, 29.70, 24.12, 15.93; ESI-MS (m/z) calcd. for $C_{19}H_{20}BrN_3O$: 385.08; Found: 386.10 $[M+H]^+$, 387.09 $[M+2]^+$; IR (neat): ν ($cm^{-1}$) 3142 (=CH str., triazole).

### *3.3 Biochemical inhibition of PfFP-2*

#### *3.3.1 Enzyme kinetics*

A construct of *Pf*FP-2 was kindly gifted by Dr. K. C. Pandey, National Institute of Malaria Research, ICMR, India. The *Pf*FP-2 was purified and refolded as described previously [36].

Inhibition of *Pf*FP-2 by **JMI-105** and **JMI-346** was observed by spectrofluorometer. Recombinant *Pf*FP-2 (25ng) was incubated for 30 min with **JMI-105** and **JMI-346** at different concentrations (1, 5, 7.5, 10, 12.5, 17.5, 20, 22.5 and 25µM) in 100 mM sodium acetate (pH 5.5) with 8 mM DTT. *Pf*FP-2 substrate Z-Phe-Arg-AMC was added just before the measurement. Samples were measured for 10 min at RT at Ex= 355 nm and Em= 460 nm to calculate the percentage of hydrolysis of peptide substrate Z-Phe-Arg-AMC substrate which reflects the percent inhibition of *Pf*FP-2. Experiment was done in triplicate.

### *3.3.2 Live cell imaging*

Live cell imaging (Nikon confocal microscopy) was performed to observe the *in vivo* hydrolysis of fluorogenic peptide Z-Phe-Arg-AMC. Briefly, synchronized trophozoite stage parasites ($10^8$ cells/ ml) were treated with **JMI-105** and **JMI-346** at 10 and 20µM concentrations at 37 ºC for 2 h. Samples were loaded with peptide substrate Z-Phe-Arg-AMC (100 µM) for 15 min at 37 ºC. Samples were washed and re-suspended with incomplete RPMI. Live cell images were captured under band pass filter at 355-460 nm with 100X objective (oil immersion). NIS element software was used to calculate mean gray intensity value [37]. Experiment was done in duplicate. Graph showed representative figures only.

### *3.3.3 Hemoglobin degradation assay*

Inhibition of *Pf*FP-2 by **JMI-105** and **JMI-346** was checked by SDS-PAGE and spectrophotometer [38, 39]. Briefly, **JMI-105** and **JMI-346** at different concentrations (1, 5, 12.5 and 25µM) were incubated with recombinant *Pf*FP-2 for 2 hr at 37ºC. Samples were then incubated with native Hb (10µg) presence and absence of **JMI-105** and **JMI-346** in 100mM sodium acetate buffer (pH 5.5) to observe the hydrolysis of native Hb. Samples were taken for both SDS-PAGE as well as spectrophotometer analysis. Absorbance intensity was taken at 410 nm (Thermo scientific, Varioskan). Experiment was done in duplicate and data were expressed as mean ± SD.

### *3.3.4 Surface Plasmon Resonance (SPR)*

SPR technique was used to determine the **JMI-105** and **JMI-346** interaction with *Pf*FP-2. SPR was done by using Auto Lab Esprit SPR. Briefly, surface of nickel charged NTA SPR chip was immobilized with 10µM concentration of *Pf*FP-2. Different concentrations (1, 10, 25, 50,

75μM) of **JMI-105** and **JMI-346** were injected over the chip surface for the interaction analysis. Association and dissociation time of 300 and 150 s was fixed. For immobilization and binding, HEPES buffer was used as solutions. NaOH solution (50mM) was used for regeneration of surface of the sensor chip. Data were evaluated by using Auto Lab SPR Kinetic Evaluation software.

### *3.3.5 Parasite culture*

Chloroquine sensitive ($CQ^S$) (3D7) and resistant ($CQ^R$) (RKL-9) *P. falciparum* strains were cultured in recently collected donor erythrocytes in complete RPMI based malaria culture medium (CMCM) according to Malaria Research and Reference Reagent Resource Center (MR4) guidelines [40]. Thin blood smears stained with Giemsa were prepared for routine monitoring. Synchronization of parasite stage was done with the help of sorbitol for the selection of rings and percoll for the selection of trophozoites.

### *3.3.6 Hemozoin Assay*

Hemozoin assay was done to quantify the monomeric heme by the method described previously [39]. Briefly, ring-stage parasites (synchronized, 6% parasitemia) were incubated with **JMI-105** and **JMI-346** at 1, 5, 12.5, 25 and 50μM concentrations. Treated samples were applied in triplicate into 96-well flat bottom microtitre plate. After 30 h of post treatment, samples were incubated with 2.5% SDS in 0.1 M sodium bicarbonate (pH 8.8) at RT for 30 min. Centrifugation was done and pellet suspended in 5% SDS and 50mM NaOH. Samples were incubated for 30 min. Absorbance was taken at 405/750 nm for the quantification of monomeric heme.

### *3.3.7 SYBR green I based fluorescence assay*

DNA-specific dye SYBR green I (Invitrogen, Carlsbad, USA) was used to perform growth inhibition assay to calculate the inhibitory effect of 21 compounds against parasite *P. falciparum* 3D7 [41]. Out of 21 compounds, **JMI-105** and **JMI-346** were selected for further study. Initially, parasites (3D7 and RKL-9 strains of *P. falciparum*) at trophozoite stage with 1% parasitemia and 2% hematocrit incubated with different concentrations (1μM-100μM) of **JMI-105** and **JMI-346**; parasites without treatment were used as negative control. Samples were seeded in 96 well microtiter plates and incubated at 37$^{o}$C for one cycle of parasite growth.

The fluorescence intensity was observed at Ex=485nm and Em=530nm spectrum. Giemsa staining was done to analyze morphological changes. Percentage growth inhibition was estimated: % Inhibition = [1 - % Parasitemia (Treatment) / % Parasitemia (Untreated Control)] *100. Data were expressed as mean ± SD. The half maximal inhibition concentration ($IC_{50}$) values of **JMI-105** and **JMI-346** were determined (Graph Pad Prism 8 software).

### *3.3.8 Blood stage specific effect*

Blood stage specific effect of **JMI-105** and **JMI-346** on 3D7 *P. falciparum* was performed as described previously [42]. Briefly, synchronized ring stage parasites of 0.8% parasitemia and 2% hematocrit were treated with **JMI-105** and **JMI-346** at $IC_{50}$ concentration in a complete RPMI-1640 medium and seeded in 96-well flat bottom microtiter plates respectively. Parasite culture was incubated and monitored upto 56 hr post treatment at 37°C. Giemsa-stained slides were made in duplicate to analyze morphological changes with the help of light microscope (Olympus).

### *3.3.9 Hemolytic activity*

Hemolysis assay was done to observe the effect of **JMI-105** and **JMI-346** compounds on human RBCs [43]. In brief, RBCs suspension 10% (v/v) washed with 1×PBS (pH 7.4) and resuspended again in 1×PBS. Suspension was treated with **JMI-105** and **JMI-346** at 1, 5, 12.5, 25 and 50µM concentrations at 37°C for 2 hr. The samples were centrifuged and absorbance of supernatant was taken at 415 nm to obtain percentage of RBCs lysis. Triton X-100 with 1% (v/v) was used as a positive control. Percentage of RBCs lysis was calculated as: % RBCs lysis = ($OD_{415nm}$ sample− $OD_{415nm}$ PBS) / ($OD_{415nm}$ Triton X-100 1%− $OD_{415nm}$ PBS).

### *3.3.10 Cytotoxicity assay*

Colorimetric MTT assay was performed to check the cytotoxicity of **JMI-105** and **JMI-346** towards human embryonic kidney (HEK293) cells [44]. HEK293 cells were cultured in DMEM media enriched with 10% FBS and 1% penicillin, streptomycin solution at 37 °C in a humidified atmosphere of 5% $CO_2$. A total of $1\times10^4$ HEK293 cells were seeded in triplicate in 96-well plate and incubated for 24 h in a $CO_2$ incubator. The cells were treated with **JMI-105** and **JMI-346** at 5-200µM concentrations for 48 h at 37°C. Freshly prepared MTT (5 mg/mL) was supplied to the samples and incubated at 37°C for 4-5 h. DMSO was added to solubilize

the formazan crystals. Microplate ELISA reader (Bio-Rad, USA) was used for taking absorbance at 570 nm and all the experiments were done in triplicate.

### *3.3.11 In vivo antimalarial activity*

The *in vivo* antimalarial activity of **JMI-105** was evaluated as reported earlier [45, 46]. Briefly, in each group four mice were taken and infected with $1\times10^7$ *P. berghei* ANKA diluted with sterile 1xPBS and injected intra-peritoneally. Thin smears were made from the tail blood of mice to check the infection. Post infection, *P. berghei* infected mice administered intraperitoneally with **JMI-105** with the dose of 30mg/Kg and 100mg/Kg body weight, daily for eight consecutive days post infection. Mice treated with 1xPBS were kept as vehicle control. Thin blood smears were made from day 1 up to day 8 to count the parasitemia and mice were observed upto 18 days for calculating mean survival time.

### *3.3.12 Statistical analysis*

To analyze the mean values obtained for the treatment and control, one-way analysis of variance (ANOVA) was used. Dunnett's test was used to compare the treatment and control and statistical significance was set at **$P<0.01$ *vs* control; $P>0.05$= non-significant.

## 4. Conclusion

*Pf*FP-2 is known as haem metabolizing enzyme responsible for initiating the degradation of host erythrocyte hemoglobin inside the food vacuole of the parasite. There are limited numbers of drugs available to kill the *Plasmodium*, this warrants the need to develop more antimalarial drugs. In this study, virtual screening strategies followed by *in vitro* and *in vivo* validation for *P. falciparum* inhibitors were pursued. The model and screening protocols were first validated theoretically on a literature database of known *Pf*FP-2 inhibitors and used subsequently to screen the *in-house* database, a small molecules library. Finally, the screening results obtained were validated experimentally by testing the most promising hits in an *in vitro* biochemical assay against the *Pf*FP-2 and cultured *P. falciparum*. Both the identified compounds and SAR oriented derivatives of **JMI-105** were tested against *P. falciparum,* which identified **JMI-105** as the most potent among all with $IC_{50}$ value 8.8 µM. *In vitro and in vivo* inhibition of proteolytic cleavage of peptide substrate Z-Phe-Arg-AMC by *Pf*FP-2 was observed. Defect in parasite growth was observed as the development of parasites was arrested at schizont stage.

Cytotoxicity results showed that 75% of HEK293 cells were viable at 200µM inhibitor concentration and hemolytic assay showed less than 5% of non-toxic nature of the tested inhibitors. The *in vivo* antimalarial efficacy on murine malaria model of **JMI-105** was evaluated and displayed significant parasitemia reduction up to 8 days. Conclusively, the potential inhibitor (**JMI-105**) identified from *in-house* library might be significant potential lead against *Pf*FP-2, and can be further evaluated in drug design and development efforts for malaria.

## 5. Acknowledgements

MA gratefully acknowledges the financial support in the form of Core Research Grant from Science & Engineering Research Board (SERB), Govt. of India (Project No. CRG/2018/003967). SS is a recipient of National Bioscientist award. SS is acknowledging Drug and Pharmaceuticals Research Programme (DPRP) (Project No. P/569/2016-1/TDT) and DST-SERB (Project No. CRG/2019/002231). AU is a recipient of Senior Research Fellowship from ICMR (Fellowship/48/2019-ECD-II). VS is a recipient of SERB-NPDF (PDF/2017/001525) from DST, Government of India. Iram Irfan acknowledges DST for fellowship under women scientist scheme (WOS-A) File no: SR/WOS-A/CS-116/2018. Authors acknowledge the support from AIRF Jawaharlal Nehru University for Live cell imaging. We are thankful to Dr. K. C. Pandey for providing construct of *Pf*FP-2 and National Institute of Malaria Research for providing RKL-9 chloroquine resistant line of *P. falciparum*. The funders had no role in study design, data collection and analysis, decision to publish, or preparation of the manuscript.

## 6. Conflict of Interest

The authors declare that they have no conflict of interest.

## Supporting Information

Virtual screening, ADME, docking results, growth inhibition data and Spectra of SAR derivatives.

**Author's contributions**

M.A. and S.S. designed the project and optimized the experiments, interpreted the data and wrote the manuscript; A.U. and M.A. screened, synthesized and characterized hit compounds and their SAR derivatives; I.I. helped in interpretation of spectral data. V.S. and A.U. performed all the biological experiments; T.M. and M.I.H. helped in performing simulation study; M.A. and S.S. provided funding acquisition and aided administrative processing. All the authors approved and reviewed the final version of the manuscript.

**Ethics statement**

SS lab, Special Center for Molecular Medicine, JNU, New Delhi has been approved by the Institutional Biosafety committee for all the experiments of this manuscript including *in vitro* culture of *P. falciparum* and *in vivo* evaluation of compounds under the guidelines of animal ethics committee, JNU.

## References


1. B. Aneja, B. Kumar, M.A. Jairajpuri, M. Abid, A structure guided drug-discovery approach towards identification of Plasmodium inhibitors, RSC advances 6(22) (2016) 18364-18406.
2. B. Kumar, T. Mohammad, A. Uddin, A. Hussain, A. Islam, F. Ahmad, M.F. Alajmi, S. Singh, K.C. Pandey, M.I. Hassan, Targeting metacaspase-3 from Plasmodium falciparum towards antimalarial therapy: A combined approach of in-silico and in-vitro investigation, Journal of Biomolecular Structure and Dynamics (just-accepted) (2019) 1-16.
3. I.M. Medana, G.D. Turner, Human cerebral malaria and the blood–brain barrier, International journal for parasitology 36(5) (2006) 555-568.
4. E.J. Walker, G.M. Peterson, J. Grech, E. Paragalli, J. Thomas, Are we doing enough to prevent poor-quality antimalarial medicines in the developing world?, BMC public health 18(1) (2018) 630.
5. V. Singh, R.S. Hada, A. Uddin, B. Aneja, M. Abid, K.C. Pandey, S. Singh, Inhibition of Hemoglobin Degrading Protease Falcipain-2 as a Mechanism for Anti-Malarial Activity of Triazole-Amino Acid Hybrids, Curr Top Med Chem 20(5) (2020) 377-389.
6. W.H. Organization, World malaria report 2019, (2019).

7. M.H. Gelb, Drug discovery for malaria: a very challenging and timely endeavor, Current opinion in chemical biology 11(4) (2007) 440-445.
8. C. Nsanzabana, Resistance to artemisinin combination therapies (ACTs): do not forget the partner drug!, Tropical medicine and infectious disease 4(1) (2019) 26.
9. K.C. Pandey, P.S. Sijwali, A. Singh, B.-K. Na, P.J. Rosenthal, Independent intramolecular mediators of folding, activity, and inhibition for the Plasmodium falciparum cysteine protease falcipain-2, Journal of Biological Chemistry 279(5) (2004) 3484-3491.
10. I.D. Kerr, J.H. Lee, C.J. Farady, R. Marion, M. Rickert, M. Sajid, K.C. Pandey, C.R. Caffrey, J. Legac, E. Hansell, Vinyl sulfones as antiparasitic agents and a structural basis for drug design, Journal of Biological Chemistry 284(38) (2009) 25697-25703.
11. D.E. Goldberg, A. Slater, A. Cerami, G.B. Henderson, Hemoglobin degradation in the malaria parasite Plasmodium falciparum: an ordered process in a unique organelle, Proceedings of the National Academy of Sciences 87(8) (1990) 2931-2935.
12. C. Lehmann, A. Heitmann, S. Mishra, P.-C. Burda, M. Singer, M. Prado, L. Niklaus, C. Lacroix, R. Ménard, F. Frischknecht, A cysteine protease inhibitor of plasmodium berghei is essential for exo-erythrocytic development, PLoS pathogens 10(8) (2014).
13. P.M. Melo, S.E.C. Maluf, M.F. Azevedo, T. Paschoalin, A. Budu, P. Bagnaresi, F. Henrique-Silva, A. Soares-Costa, M.L. Gazarini, A.K. Carmona, Inhibition of Plasmodium falciparum cysteine proteases by the sugarcane cystatin CaneCPI-4, Parasitology international 67(2) (2018) 233-236.
14. J. Liu, E.S. Istvan, I.Y. Gluzman, J. Gross, D.E. Goldberg, Plasmodium falciparum ensures its amino acid supply with multiple acquisition pathways and redundant proteolytic enzyme systems, Proceedings of the National Academy of Sciences 103(23) (2006) 8840-8845.
15. Y. Fagnidi, B. Toi, E. Megnassan, In silico design of Plasmodium falciparum cysteine protease falcipain 2 inhibitors with favorable pharmacokinetic profile, J Anal Pharm Res 7(3) (2018) 298-309.
16. B.K. Shoichet, Virtual screening of chemical libraries, Nature 432(7019) (2004) 862-865.
17. P.A. Ravindranath, S. Forli, D.S. Goodsell, A.J. Olson, M.F. Sanner, AutoDockFR: advances in protein-ligand docking with explicitly specified binding site flexibility, PLoS computational biology 11(12) (2015).
18. X. Fradera, K. Babaoglu, Overview of methods and strategies for conducting virtual small molecule screening, Current protocols in chemical biology 9(3) (2017) 196-212.
19. P.J. Rosenthal, Antimalarial drug discovery: old and new approaches, Journal of Experimental Biology 206(21) (2003) 3735-3744.
20. P.V. Desai, A. Patny, J. Gut, P.J. Rosenthal, B. Tekwani, A. Srivastava, M. Avery, Identification of novel parasitic cysteine protease inhibitors by use of virtual screening. 2. The available chemical directory, Journal of medicinal chemistry 49(5) (2006) 1576-1584.
21. O. Trott, A.J. Olson, AutoDock Vina: improving the speed and accuracy of docking with a new scoring function, efficient optimization, and multithreading, Journal of computational chemistry 31(2) (2010) 455-461.
22. D.S. Biovia, Discovery Studio Modeling Environment, release 4.5; Dassault Systèmes: San Diego, 2015, There is no corresponding record for this reference.[Google Scholar].
23. W. DeLano, The PyMOL Molecular Graphics System (DeLano Scientific, Palo Alto, CA), 2002.

24. A. Daina, O. Michielin, V. Zoete, SwissADME: a free web tool to evaluate pharmacokinetics, drug-likeness and medicinal chemistry friendliness of small molecules, Scientific reports 7 (2017) 42717.
25. L. Zhang, H. Ai, W. Chen, Z. Yin, H. Hu, J. Zhu, J. Zhao, Q. Zhao, H. Liu, CarcinoPred-EL: novel models for predicting the carcinogenicity of chemicals using molecular fingerprints and ensemble learning methods, Scientific reports 7(1) (2017) 1-14.
26. R.B. Jacob, T. Andersen, O.M. McDougal, Accessible high-throughput virtual screening molecular docking software for students and educators, PLoS computational biology 8(5) (2012).
27. J.C. de Carvalho Gallo, L. de Mattos Oliveira, J.S.C. Araújo, I.B. Santana, M.C. dos Santos Junior, Virtual screening to identify Leishmania braziliensis N-myristoyltransferase inhibitors: pharmacophore models, docking, and molecular dynamics, Journal of molecular modeling 24(9) (2018) 260.
28. E. Lindahl, B. Hess, D. Van Der Spoel, GROMACS 3.0: a package for molecular simulation and trajectory analysis, Molecular modeling annual 7(8) (2001) 306-317.
29. M. Sobol, Drug-like properties: Concepts, structure design and methods from ADME to toxicity optimization [Book Review], Chemistry in Australia (Jul/Aug 2018) (2018) 28.
30. W.L. DeLano, Unraveling hot spots in binding interfaces: progress and challenges, Current opinion in structural biology 12(1) (2002) 14-20.
31. G.M. Morris, R. Huey, W. Lindstrom, M.F. Sanner, R.K. Belew, D.S. Goodsell, A.J. Olson, AutoDock4 and AutoDockTools4: Automated docking with selective receptor flexibility, Journal of computational chemistry 30(16) (2009) 2785-2791.
32. F. Naz, F.I. Khan, T. Mohammad, P. Khan, S. Manzoor, G.M. Hasan, K.A. Lobb, S. Luqman, A. Islam, F. Ahmad, Investigation of molecular mechanism of recognition between citral and MARK4: A newer therapeutic approach to attenuate cancer cell progression, International journal of biological macromolecules 107 (2018) 2580-2589.
33. B. Aneja, M. Azam, S. Alam, A. Perwez, R. Maguire, U. Yadava, K. Kavanagh, C.G. Daniliuc, M.M.A. Rizvi, Q.M.R. Haq, Natural product-based 1, 2, 3-triazole/sulfonate analogues as potential chemotherapeutic agents for bacterial infections, ACS omega 3(6) (2018) 6912-6930.
34. M.M. Masood, P. Hasan, S. Tabrez, M.B. Ahmad, U. Yadava, C.G. Daniliuc, Y.A. Sonawane, A. Azam, A. Rub, M. Abid, Anti-leishmanial and cytotoxic activities of amino acid-triazole hybrids: Synthesis, biological evaluation, molecular docking and in silico physico-chemical properties, Bioorganic & medicinal chemistry letters 27(9) (2017) 1886-1891.
35. B. Aneja, R. Arif, A. Perwez, J.V. Napoleon, P. Hasan, M.M.A. Rizvi, A. Azam, M. Abid, N-Substituted 1, 2, 3-Triazolyl-Appended Indole-Chalcone Hybrids as Potential DNA Intercalators Endowed with Antioxidant and Anticancer Properties, ChemistrySelect 3(9) (2018) 2638-2645.
36. P.S. SIJWALI, B.R. SHENAI, J. GUT, A. SINGH, P.J. ROSENTHAL, Expression and characterization of the Plasmodium falciparum haemoglobinase falcipain-3, Biochemical Journal 360(2) (2001) 481-489.
37. R. Korde, A. Bhardwaj, R. Singh, A. Srivastava, V.S. Chauhan, R.K. Bhatnagar, P. Malhotra, A prodomain peptide of Plasmodium falciparum cysteine protease (falcipain-2) inhibits malaria parasite development, Journal of medicinal chemistry 51(11) (2008) 3116-3123.
38. S.-U. Moon, J.-M. Kang, T.-S. Kim, Y. Kong, W.-M. Sohn, B.-K. Na, Plasmodium vivax: collaborative roles for plasmepsin 4 and vivapains in hemoglobin hydrolysis, Experimental parasitology 128(2) (2011) 127-132.

39. T.T. Men, N.T. Huy, M.N. Shuaibu, K. Hirayama, K. Kamei, A simple and inexpensive haemozoin-based colorimetric method to evaluate anti-malarial drug activity, Malaria journal 11(1) (2012) 272.
40. F.A. Mphande, U. Ribacke, O. Kaneko, F. Kironde, G. Winter, M. Wahlgren, SURFIN 4.1, a schizont-merozoite associated protein in the SURFIN family of Plasmodium falciparum, Malaria journal 7(1) (2008) 116.
41. M. Makler, J. Ries, J. Williams, J. Bancroft, R. Piper, B. Gibbins, D. Hinrichs, Parasite lactate dehydrogenase as an assay for Plasmodium falciparum drug sensitivity, The American journal of tropical medicine and hygiene 48(6) (1993) 739-741.
42. C. Moneriz, J. Mestres, J.M. Bautista, A. Diez, A. Puyet, Multi-targeted activity of maslinic acid as an antimalarial natural compound, The FEBS journal 278(16) (2011) 2951-2961.
43. B.C. Evans, C.E. Nelson, S.Y. Shann, K.R. Beavers, A.J. Kim, H. Li, H.M. Nelson, T.D. Giorgio, C.L. Duvall, Ex vivo red blood cell hemolysis assay for the evaluation of pH-responsive endosomolytic agents for cytosolic delivery of biomacromolecular drugs, JoVE (Journal of Visualized Experiments) (73) (2013) e50166.
44. F.A. Wani, Amaduddin, B. Aneja, G. Sheehan, K. Kavanagh, R. Ahmad, M. Abid, R. Patel, Synthesis of Novel Benzimidazolium Gemini Surfactants and Evaluation of Their Anti-Candida Activity, ACS omega 4(7) (2019) 11871-11879.
45. D. Knight, W. Peters, The antimalarial activity of N-benzyloxydihydrotriazines: I. The activity of clociguanil (BRL 50216) against rodent malaria, and studies on its mode of action, Annals of Tropical Medicine & Parasitology 74(4) (1980) 393-404.
46. S. Ounjaijean, M. Kotepui, V. Somsak, Antimalarial Activity of Tinospora baenzigeri against Plasmodium berghei-Infected Mice, Journal of tropical medicine 2019 (2019).
47. J.-F. Wang, K.-C. Chou, Insight into the molecular switch mechanism of human Rab5a from molecular dynamics simulations, Biochemical and biophysical research communications 390(3) (2009) 608-612.
48. T. Mohammad, F.I. Khan, K.A. Lobb, A. Islam, F. Ahmad, M.I. Hassan, Identification and evaluation of bioactive natural products as potential inhibitors of human microtubule affinity-regulating kinase 4 (MARK4), Journal of Biomolecular Structure and Dynamics 37(7) (2019) 1813-1829.
49. V. Gramany, F.I. Khan, A. Govender, K. Bisetty, S. Singh, K. Permaul, Cloning, expression, and molecular dynamics simulations of a xylosidase obtained from Thermomyces lanuginosus, Journal of Biomolecular Structure and Dynamics 34(8) (2016) 1681-1692.
50. F.I. Khan, M. Shahbaaz, K. Bisetty, A. Waheed, W.S. Sly, F. Ahmad, M.I. Hassan, Large scale analysis of the mutational landscape in β-glucuronidase: a major player of mucopolysaccharidosis type VII, Gene 576(1) (2016) 36-44.
51. Y. Mazola, O. Guirola, S. Palomares, G. Chinea, C. Menéndez, L. Hernández, A. Musacchio, A comparative molecular dynamics study of thermophilic and mesophilic β-fructosidase enzymes, Journal of molecular modeling 21(9) (2015) 228.
52. R.E. Hubbard, M. Kamran Haider, Hydrogen bonds in proteins: role and strength, e LS (2001).
53. R. Ettari, F. Bova, M. Zappalà, S. Grasso, N. Micale, Falcipain-2 inhibitors, Medicinal research reviews 30(1) (2010) 136-167.
54. P.J. Rosenthal, Falcipains and other cysteine proteases of malaria parasites, Cysteine Proteases of Pathogenic Organisms, Springer2011, pp. 30-48.
55. P. Malhotra, P.V. Dasaradhi, A. Mohammed, M. Hossain, S. Mukherji, M. Venkatasamy, K. Rao, G. Mishra, P. Subrayan, A. Chatterji, Use of selected amino acid-zinc complexes as anti-malarials, Google Patents, 2005.

56. J.A. Rowe, A. Claessens, R.A. Corrigan, M. Arman, Adhesion of Plasmodium falciparum-infected erythrocytes to human cells: molecular mechanisms and therapeutic implications, Expert reviews in molecular medicine 11 (2009).
57. E.L. Dahl, P.J. Rosenthal, Biosynthesis, localization, and processing of falcipain cysteine proteases of Plasmodium falciparum, Molecular and biochemical parasitology 139(2) (2005) 205-212.
58. P. Gupta, S. Mehrotra, A. Sharma, M. Chugh, R. Pandey, A. Kaushik, S. Khurana, N. Srivastava, T. Srivastava, A. Deshmukh, Exploring heme and hemoglobin binding regions of plasmodium heme detoxification protein for new antimalarial discovery, Journal of medicinal chemistry 60(20) (2017) 8298-8308.
59. S.L. Farias, M.L. Gazarini, R.L. Melo, I.Y. Hirata, M.A. Juliano, L. Juliano, C.R. Garcia, Cysteine-protease activity elicited by Ca2+ stimulus in Plasmodium, Molecular and biochemical parasitology 141(1) (2005) 71-79.
60. K.C. Pandey, S.X. Wang, P.S. Sijwali, A.L. Lau, J.H. McKerrow, P.J. Rosenthal, The Plasmodium falciparum cysteine protease falcipain-2 captures its substrate, hemoglobin, via a unique motif, Proceedings of the National Academy of Sciences 102(26) (2005) 9138-9143.
61. C. Lehmann, M.S.Y. Tan, L.E. de Vries, I. Russo, M.I. Sanchez, D.E. Goldberg, E. Deu, Plasmodium falciparum dipeptidyl aminopeptidase 3 activity is important for efficient erythrocyte invasion by the malaria parasite, PLoS pathogens 14(5) (2018) e1007031.
62. A. Semenov, J.E. Olson, P.J. Rosenthal, Antimalarial synergy of cysteine and aspartic protease inhibitors, Antimicrobial agents and chemotherapy 42(9) (1998) 2254-2258.
63. N.T. Huy, Y. Shima, A. Maeda, T.T. Men, K. Hirayama, A. Hirase, A. Miyazawa, K. Kamei, Phospholipid membrane-mediated hemozoin formation: the effects of physical properties and evidence of membrane surrounding hemozoin, PloS one 8(7) (2013).
64. A.P. Gorka, J.N. Alumasa, K.S. Sherlach, L.M. Jacobs, K.B. Nickley, J.P. Brower, A.C. De Dios, P.D. Roepe, Cytostatic versus cytocidal activities of chloroquine analogues and inhibition of hemozoin crystal growth, Antimicrobial agents and chemotherapy 57(1) (2013) 356-364.
65. N.T. Huy, K. Kamei, T. Yamamoto, Y. Kondo, K. Kanaori, R. Takano, K. Tajima, S. Hara, Clotrimazole Binds to Heme and Enhances Heme-dependent Hemolysis PROPOSED ANTIMALARIAL MECHANISM OF CLOTRIMAZOLE, Journal of Biological Chemistry 277(6) (2002) 4152-4158.
66. S.E. Francis, D.J. Sullivan Jr, Goldberg, D. E, Hemoglobin metabolism in the malaria parasite Plasmodium falciparum, Annual Reviews in Microbiology 51(1) (1997) 97-123.
67. B.L. Tekwani, L.A. Walker, Targeting the hemozoin synthesis pathway for new antimalarial drug discovery: technologies for in vitro β-hematin formation assay, Combinatorial chemistry & high throughput screening 8(1) (2005) 63-79.
68. S. Manohar, U.C. Rajesh, S.I. Khan, B.L. Tekwani, D.S. Rawat, Novel 4-aminoquinoline-pyrimidine based hybrids with improved in vitro and in vivo antimalarial activity, ACS Medicinal Chemistry Letters 3(7) (2012) 555-559.

**Highlights**

- Structure-guided virtual screening identified **JMI-105** and **JMI-346** as putative *Pf*FP-2 inhibitors.
- The anti-malarial potential of both the compounds was established using various cell-free and cell-based assays.
- No significant hemolysis or cytotoxicity towards human cells was observed suggesting their safety profile.
- **JMI-105** significantly decreased parasitemia in a murine model with *P. berghei* ANKA infection.